Aalto University
School of Chemical Engineering
Chemical, Biochemical and Materials Engineering

Woojae Lim

Deposition of indigo thin films by Langmuir-Schaefer technique

Master's Thesis
Espoo, December 11, 2018

Supervisor: Professor Päivi Laaksonen, Aalto University

Advisor: Alessandra Griffo M.Sc., Aalto University

Aalto University
School of Chemical Engineering
Chemical, Biochemical and Materials Engineering

Aalto University
School of Chemical Technology

ABSTRACT OF MASTER'S THESIS

Author:	Woojae Lim	
Title:	Deposition of indigo thin films by Langmuir-Schaefer technique	
Date:	December 11, 2018	**Pages:** vii + 55
Major:	Functional Materials	**Code:** CHEM3025
Supervisor:	Professor Päivi Laaksonen	
Advisor:	Alessandra Griffo M.Sc.	

The main purpose of this thesis is to explore an opportunity to create a conductive thin film on the substrate for organic semiconductors with non-amphiphilic molecules of indigo by Langmuir-Schaefer deposition.

The hypothesis of this study was that high surface pressure of a Langmuir film of indigo leaded to an ordered Langmuir-Schaefer film. To do the experiment, Indigo powders were dissolved in a chloroform solvent and stirred at room temperature. The substrates of glass and SiO_2 for deposition were silanized to imitate a dielectric layer between a gate and a semiconducting film. After Langmuir-Schaefer deposition, the samples were mainly characterized by ultraviolet–visible spectroscopy (UV-Vis) and atomic force microscopy (AFM).

In UV-Vis characterization, the max absorption peak of the indigo film on the glass substrate was red-shifted to 670 nm from 600 nm of indigo solution due to the hydrogen bond between indigo molecules. The max absorption peak of an indigo film was red-shifted as decreasing surface pressure of Langmuir film and/or the number of deposition cycles. The AFM characterization revealed that the thickness of indigo thin film was around 5nm. It was also found that aggregates of indigo covered the surfaces of the samples and calculated root-mean-square surface roughness lay in between 2.6 to 18 nm.

In sum, this study showed that Langmuir-Schaefer deposition succeeded in creating an indigo thin film, and low surface pressure of a Langmuir film consisting of non-amphiphilic molecules of indigo has a positive impact to have an ordered Langmuir-Schaefer film.

Keywords:	indigo dye, Langmuir deposition, organic semiconductor, surface pressure-area isotherm, Langmuir film
Language:	English

Acknowledgements

This work was conducted in the Aalto University School of Chemical Engineering Department of Chemistry and Materials Science.

First, I would like to thank my supervisor, Prof. Päivi Laaksonen, for the opportunity to write this thesis. During the entire period of this thesis, she kindly offered me invaluable suggestions and feedback to make this project go in the correct direction, and helped me to solve technical problems. I would like to thank my advisor, M. Sc. Alessandra Griffo, for teaching how to use laboratory tools I had not known. I really appreciate her effort to take a lot of AFM images and process them to achieve better images. I would like to thank Olli Casey for helping to plot UV-Vis absorption of indigo solution. I would like to thank Tia Lohtander for the tutorial of UV-Vis.

Second, I would like to appreciate my parents, sister, parents-in-law, and all relatives for sending their endless support from South Korea.

Lastly, I would like to dedicate this work to my lovely daughter and son. I would like to truly appreciate my wife for giving the endless encouragement and devotions. Words cannot describe how much I appreciate all moments of last three years with them to in Finland.

Espoo, December 11, 2018

Woojae Lim

Contents

Abbreviations and Acronyms

AFM	Atomic force microscopy
ANOVA	Analysis of variance
BCH	Bicylohexyl ($C_{12}H_{22}$)
Disperse Red 13	$C_{16}H_{17}ClN_4O_3$
HF	Hydrofluoric acid
HOMO	Highest occupied molecular orbital
H_2O_2	Hydrogen peroxide
LB deposition	Langmuir–Blodgett deposition
LB film	Langmuir–Blodgett film
LB PAN	Langmuir–Blodgett film of PAN molecules
LS deposition	Langmuir–Schaefer deposition
LS film	Langmuir–Schaefer film
LUMO	Lowest unoccupied molecular orbital
O	Oxygen
OFETs	Organic field-effect transistors
OM	Optical microscopy
OTS	Trichloro(octadecyl)silane
PAN	Poly (5-amino-1-naphthol)
Parylene C	Chemical vapor deposited poly(p-xylylene) polymers
PEDOT:PSS	Poly(3,4-ethylenedioxythiophene) polystyrene sulfonate
PVK	Poly(3-30(vinylcarbazole))
Ra	Arithmetic average of the absolute values of the profile height
Rq	Root-mean-square average of the profile height
SAMs	Self-assembled monolayers
Si	Silicon
SiO_2	Silicon dioxide
TTC	Tetratetracontane
UV-Vis	Ultraviolet–visible spectroscopy
XRD	X-ray diffraction

List of Figures

Chapter 1

Introduction

Organic semiconductors have been expected to open new generation of electronic devices for many decades due to the advantages of the conjugated polymers such as biodegradability, sustainable and low-cost fabrication, relatively a low or temperature of process, which are valuable properties for applications like flexible electronic devices and biocompatible sensors in and on the human body. [1–10] Even though brilliant achievements have been observed in inorganic electronics, inorganic semiconductors are hard to succeed in flexible devices and sensors for living beings because of a rigid physical property and health incompatibility.

Many researchers have been investigating indigo dye as an ingredient for organic semiconductors recently. It is known that people have used indigo and its derivatives as a dyeing material for 4000 years. Since the color of blue was rare to achieve, people who were members of the royal family and the nobility used them to show their power and status. [11] Indigo became popular owing to the discovery of synthetic production of indigo by the effort of a German company and chemists in the late 19th century. Indigo is one of the most consumed dyeing materials in the world, most of them seen from blue jeans. [11–16]

An enormous low solubility of indigo was the main limitation to researchers not to study it as a material having functional groups for other purposes. [17] However, recent studies of indigo and its derivatives revealed some important facts, and this attracted much attention from scientists. First, it is known that indigo has additional intermolecular hydrogen bonding compared to other normal organic materials having intermolecular interaction with van der Waals force and pi-pi interaction. Second, thin films of indigo and tyrian purple used in organic field-effect transistors showed an enormous high order of plane in growth direction without amorphous domains. [11, 18–20]

The recent results of charge mobilities of the organic semiconductors made of indigo and its derivatives are shown in Figure 1.1. These results of recent research can be grouped into two categories in terms of the method of deposition of indigo and its derivatives. One is Langmuir method using indigo and/or its derivatives having hydrocarbon chains. The other is spin coating or vacuum evaporation deposition which is not the Langmuir method. Therefore, it is unsure that Langmuir method can offer an opportunity to deposit pure indigo without hydrocarbon chains to form an ordered thin film or not.

The purpose of this thesis is to explore a possibility to use non-amphiphilic indigo dye, which does not have hydrocarbon chains, for the creation of ordered indigo thin films on the substrates by Langmuir-Schaefer method. This

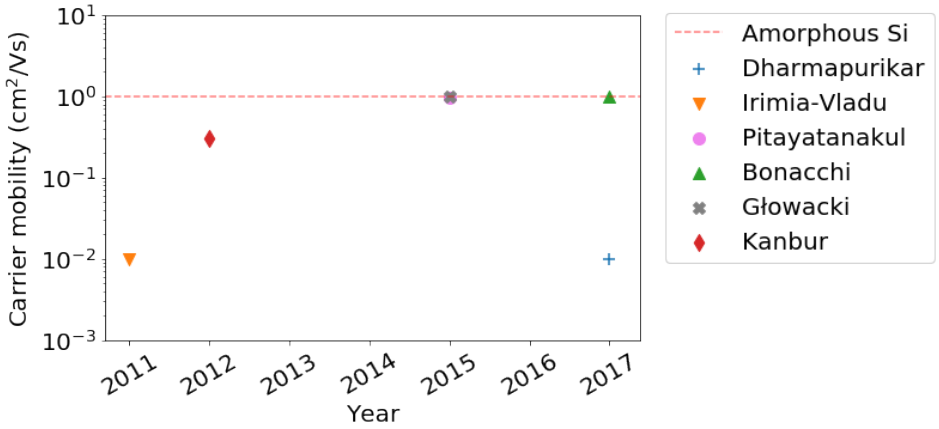

Figure 1.1. Recent results of charge the mobilities of organic field-effect transistors using indigo and its derivatives for the semiconducting layers. [10, 19, 21–24] Red dotted line drawn at 1 $cm^2V^{-1}s^{-1}$ is the charge mobility of amorphous silicon as the reference line for comparing the performance of organic semiconductor. The displayed results are the best from their electron or hole mobility were selected. Dharmapurikar et al. and Sara Bonacchi et al. deposited the semiconducting layers using spin coating deposition and Langmuir–Schaefer deposition, respectively. Rest of research group applied vacuum evaporation deposition.

research method has not tried by other research groups so that this research will contribute to broadening the horizon of indigo research for organic semiconductor. The research data in this study is collected from four sources : optical microscope, the balance of Langmuir trough, UV-Vis spectroscope, and atomic force microscope.

The paper has been organized in the following way. Chapter 2, the background and literature review part, will cover the basic information and principles about indigo, organic field effect transistors, Langmuir method, and UV-Vis and AFM characterizations as well as recent studies. Chapter 3, the experimental part, will describe actual experiment details such as the creation of indigo solution, the pre-treatment of substrates, and the procedures of Langmuir deposition. Chapter 4, the results and discussion part, will report the main findings and analysis of Langmuir isotherms, optical microscopy, UV-Vis, and AFM characterization. Chapter 5, the conclusion part, will summarize the entire thesis.

Chapter 2

Background and literature review

2.1 Unique structure of indigo molecule

Indigo is known as an extremely insoluble material in both polar and non-polar solvent due to its unique structure. As shown in Figure 2.1, the carbonyl group in the molecule forms a hydrogen bonding with an adjacent hydrogen atom from its amine group. [14] The structure of indigo is fairly symmetric so that dipole moments are offset by each other.

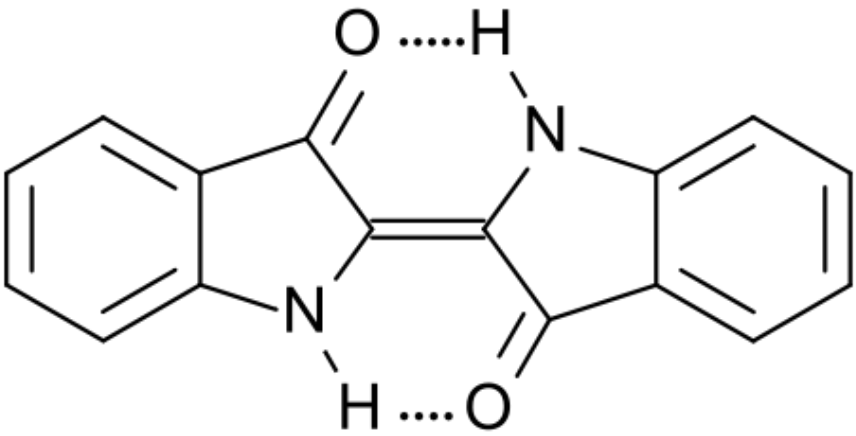

Figure 2.1. The structure of an indigo molecule. The molecule has aromatic hydrocarbons on each side and two carbonyl and amine groups are placed in the middle, symmetrically. The hydrogen bond between amine and carbonyl groups displayed the dotted line is the reason of strong stability. This figure was referred from the webpage "https://pubchem.ncbi.nlm.nih.gov".

2.2 Organic field-effect transistors (OFETs)

2.2.1 Structure of OFET

The general structure of an OFET is shown in Figure 2.2. Basically, OFETs inherited its structure from a thin-film silicon transistor consisting of three electrodes that includes a source, a drain and gate electrodes, and an insulating

layer in between the gate and a semiconducting layer that separates them. In OFETs, the semiconducting layer is composed of a thin film of organic molecules, which connects two drain and source electrodes. [25–28]

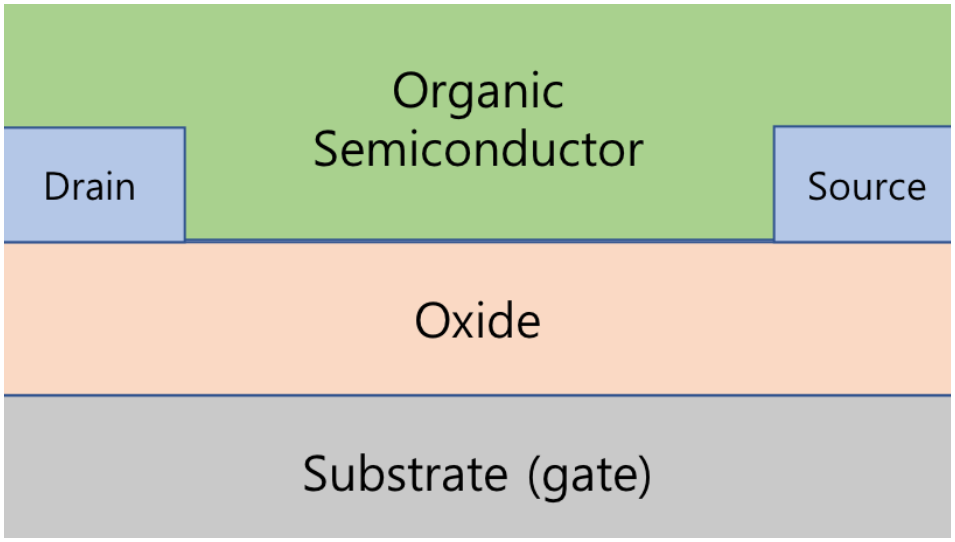

Figure 2.2. Schematic image of an OFET.

2.2.2 Working principle of OFET

The general working principle of OFETs have been explained in review papers. [25, 29] An OFET behaves as a capacitor, and its function is focused on using as a signal amplifier or an on/off switch. When the gate applied an electric field, it changes the conductivity of the semiconducting layer so that flow of electric current from the source to the drain can be controlled. The phenomenon caused by the applied electric field is called the field effect. This plays a role analogous to a water tap controlling the amount of water the flows out. [26–28]

Factors affecting OFETs performance are comprehensively explained by Wang et al. [25] In their paper, the factors are categorized into two groups; one factor originated from semiconducting pi-conjugated systems and the other from device physics.

In the pi-conjugated system, the efficient charge transport is proportional to the electron mobility of a semiconductor. As a result, it is relevant to take into account two parameters that are strongly related to the mobility; the transfer integral and the reorganization energy. The transfer integral indicates the energy difference between the highest occupied molecular orbital (HOMO) and the lowest unoccupied molecular orbital (LUMO), and the gap is strongly linked to the degree of the pi-bonds with nearby molecules. The reorganization energy is the energy loss of a charge carrier happening during the movement through a molecule.

The paper further noted that the arrangement of the organic molecules significantly affects the transfer integral and the reorganization energy. [25] Four different ways of packing were given in Figure 2.3. The top left image (a) shows face to edge packing without pi-pi overlap. The top right image (b) shows face to face packing. The bottom left image (c) presents one-dimensional lamellar pi-stacking. The bottom right image (d) is called lamellar packing that has a two-dimensional pi-stacking. According to the general effect of the two parameters, the last one is thought to be the most efficient one due to the shortest route for the charge carriers and the maximization of the transfer integrals.

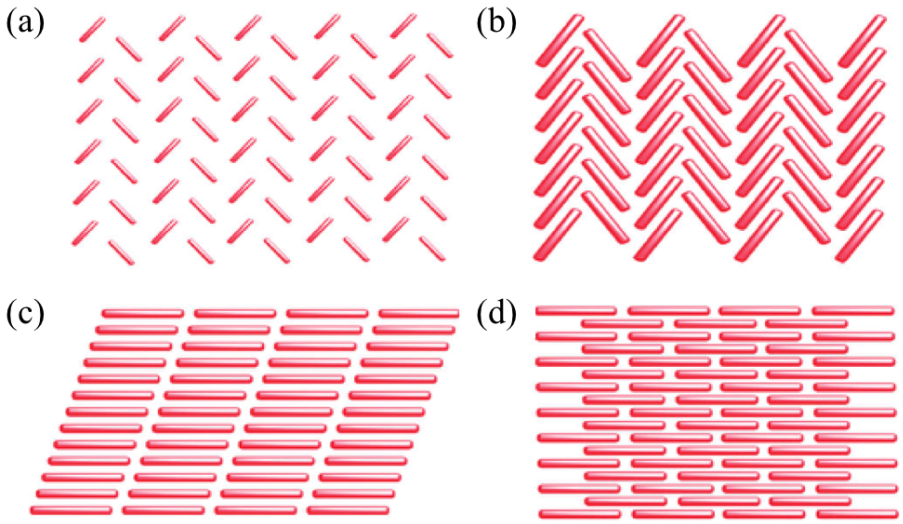

Figure 2.3. Four different arrangements of the organic molecules (a) Face to edge packing with no pi-pi overlap (b) Face to edge with pi-pi overlap (c) Lamellar 1-dimension pi-stacking (d) Lamellar, 2- dimensions pi-stacking. These images were originated from two different articles [30, 31]

In device physics, selecting suitable materials for an insulating layer is crucial for several reasons. A greater dielectric constant of insulating layer offers a more integrated circuit, less driving voltage, and less the dimension of the device. [25] The physical and chemical properties of the insulating layer directly affect the structure and the morphology of the semiconducting layer.

The packing direction of the molecules in the semiconducting film affects the efficiency of charge transportation between the source and the drain electrodes. In Figure 2.4, image (a) displays that the conjugation and the pi-pi stacking directions are faster than the interchain direction. Hence, If the pi-staking direction as shown in Figure 2.4 (b) is aligned with the direction of the current, the packing is much more effective for charge transportation than the interchain direction as shown in Figure 2.4 (c)

With respect to checking the performance of an OFET, three values such as

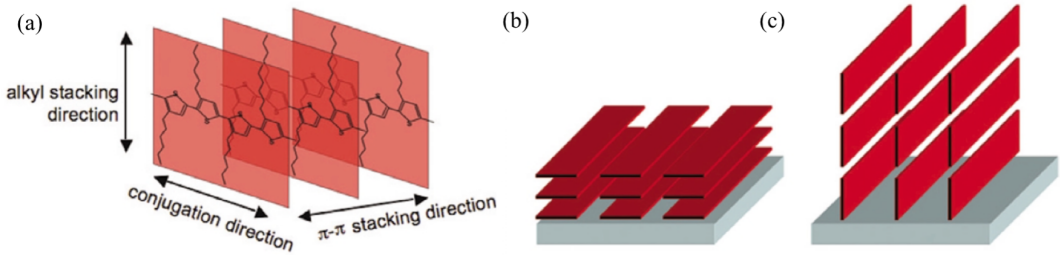

Figure 2.4. (A) Two faster charge transport directions: the conjugation and the pi-pi stacking directions, slower charge transport direction : interchain direction (B) Face-on and (C) edge-on orientation of the polymer molecules on the substrates. The face-on orientation is slow due to the alkyl stacking direction aligned with the current flow direction. These images were referred from an article [32]

the carrier mobility (μ), the on/off current ratio, and the threshold voltage (V_{th}) are considered in most cases. The carrier mobility exceeding over 1 $cm^2V^{-1}s^{-1}$ is thought of as the benchmark for organic semiconductors, which is similar to amorphous Si. The on/off current ratio between the maximum on-state to the minimum off-state represents a leakage current, which means that higher on/off current ratio leads to less current leakage. The threshold voltage is the minimum gate voltage to create a minimum conductive path from the source to the drain. [25, 33]

2.2.3 Advantages of OFETs and their applications

Organic semiconductors have several advantages compared to inorganic semiconductors. They can be fabricated in a sustainable process without using toxic chemicals such as hydrofluoric acid (HF), Hydrogen Peroxide (H_2O_2) so that the amount of waste of electronics can be reduced. Some of OFETs made of biodegradable components could be used safely in the human body, which opens up new possibilities for new medical applications. The general process of the fabrication of OFETs works in room temperature or relatively low temperature compared to that of a traditional semiconductor manufacturing, so potentially leading to process cost saving. [11] A lot of research group have investigated and mentioned the possible applications of OFETs such as RF-ID tags for smart packaging, flexible led display and solar cells for foldable mobile phones and electric cars, and fabricated on the textile for smart clothing. [34–38]

2.2.4 Recent studies of OFETs using indigo and indigo derivatives

Dharmapurikar et al. reported in 2017 that they had fabricated OFET devices with isoindigo co-polymers thin film by spin coating method on the SiO_2 that was the gate insulating layer thermally grown on the Si water substrate. Among the devices they created, poly(reg-iInd-DT) showed the highest charge carrier mobility 1.0x10^{-2} cm^{2}V^{-1}s^{-1}. However, the rest of devices using other polymers showed less carrier mobility. [10]

Irimia-Vladu et al. created a few OFETs consisting of an indigo derivative semiconducting film deposited on shellac resin substrates by means of the evaporation method in 2011. They mentioned for the first time the possibility of indigo as a semiconducting film for ambipolar OFETs. They reported their results that the measured mobilities of the electron and hole are around 1.0x10 $^{-2}$cm^{2}V^{-1}s^{-1} and 5.0x10^{-3} to 1.0x10^{-2} cm^{2}V^{-1}s^{-1}, respectively. The hole mobility is smaller than that of amorphous silicon ($\mu_p \simeq 1$ cm^{2}V^{-1}s^{-1}). The threshold voltage ranged from –1.5 to –3 V for holes and 4.5 to 7 V for electrons. [19]

Pitayatanakul et al. deposited indigo derivatives by vacuum evaporation to produce OFETs in 2015. It consisted of the top insulation layer of polychloroparaxylylene (Parylene C), poly(3,4-ethylenedioxythiophene): poly-(stylenesulfonate) (PEDOT:PSS) below the Parylene C as a gate electrode on top of a polyethylenenaphtalate (PEN) substrate. In this paper, they paid attention to halogen and phenyl substituted indigo derivatives to enhance ambipolar properties. The highest recording of mobilities of the hole and electron of both the diiodo-indigo and the diphenyl-indigo were 0.42/0.85 and 0.56/0.95 cm^{2}V^{-1}s^{-1}, respectively. They concluded that the reason for the improvement is that the phenyl substituents brought a hybrid structure of face-to-edge packing and lamellar packing. [21]

Three different research groups investigated different indigo derivatives with a various deposition methods. Measured hole mobilities of indigo derivatives laid in between 0.3 and 1.5 cm^{2}V^{-1}s^{-1}. In order to increase an electron mobility, deposition of a multilayer or enhancement of close pi-stacking was utilized. [22–24]

2.3 Self-assembled monolayers (SAMs)

2.3.1 Structure of self-assembled monolayers and its principle

A self-assembled monolayer (SAM) is the functional group of organic molecules that have arranged on the surface by a chemisorption. The molecule of SAM consists of three parts such as a head group, a backbone chain, and a terminal group. Figure 2.5 shows the schematic illustration of SAM on the substrate.

The phenomenon of self-assembly happens spontaneously due to the fact that the head groups of the adsorbate molecules have a specific affinity for a substrate. So they decrease the surface free-energy of the substrate by replacing pre-adsorbed organic materials on the surface. The backbone chain linked both the head and the terminal groups is stabilized by means of electrostatic forces with other backbone chains to reduce their own energy so that it affects the orientation and packing density of the molecules. It is known that the direction of backbone chains are affected by the relationship between the substrate and the head group as well as the interactions of backbone chains. The terminal group facing the outer surface is responsible for surface energy and topography of the monolayer. [29, 39–42]

Self-assembled monolayers (SAMs) have been investigated by research groups because SAMs offer a simple way to modify the properties of a surface precisely for different applications. [42] From a making OFETs perspective, SAMs provide a dielectric thin film to isolate the channel of an OFFT from the gate electrode. The morphology and structural order of the channel is affected by the surface property of the dielectric film. A few research groups showed that it is also possible to insert a SAM between the drain and source to control the Mott–Schottky barrier, which is the potential energy barrier between the work function of the electrodes and the HOMO or LUMO level of the organic semiconductor for enhancing a charge injection. [43–46] From a biocompatible purpose perspective, SAMs are especially beneficial due to the fact that the monolayer is able to be disassembled by the metabolism of the body. [47]

It is known that the thickness of a SAM is in the scale of a few nanometers. It is possible to increase the height of SAMs between in the range of between 10 and 100 nm by patterning techniques like scanning probe and microcontact printing. [42]

Trichloro(octadecyl)silane(OTS) is one of materials that is broadly used as a source molecule for a SAM due to offering stable layer and being replicated to have certain surface properties. [48–51] It has been reported that the molecules of OTS form a SAM that is stable and semicrystalline structure because OTS molecules bond with a hydroxy group strongly, and their partial cross-linking between nearby molecules results in Si-O-Si network of the head groups. [29, 39] It has been shown that the backbone chains are tilted, and its density and order can be controlled by preparation temperature. [52, 53]

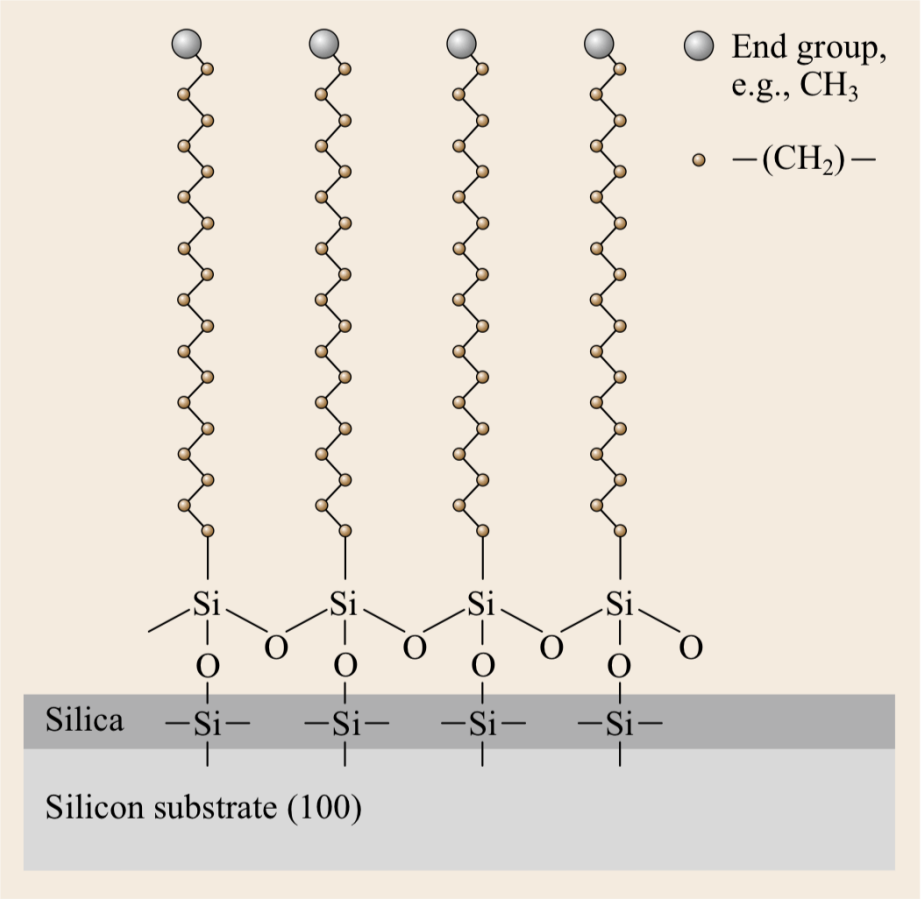

Figure 2.5. A schematic image of OTS molecules on SiO_2. When the polar head group ($SiCl_3$–) of OTS molecules meet hydroxyl functional group (OH) on silicon dioxide, oxygen atoms of OH become hydrochloric acid with chlorine atoms of the polar head groups. The silicons of the polar head group anchor to the SiO_2 surface. This figure was taken from the handbook of nanotechnology. [39]

2.4 Langmuir trough

2.4.1 Theory of Langmuir deposition

Numerous research groups used various techniques to create and investigate thin films on the substrates. Among them, Langmuir-Schaefer (LS) is the one of techniques to deposit an organic film that consists of a monolayer of molecules from the liquid-air interface onto a solid substrate. [54]

The LS-technique has several appealing features for coating one-layer film. First, the film thickness on a substrate can be controlled precisely. Second, deposition of a multilayer with different composition is possible. Third, transferring a homogeneous film on the solid substrate is possible. [55, 56]

The Langmuir trough is the instrument used to fabricate Langmuir-Blodgett

or Langmuir-Schaefer film. The instrument is composed of several components. The Schematic illustration is shown by Figure 2.6

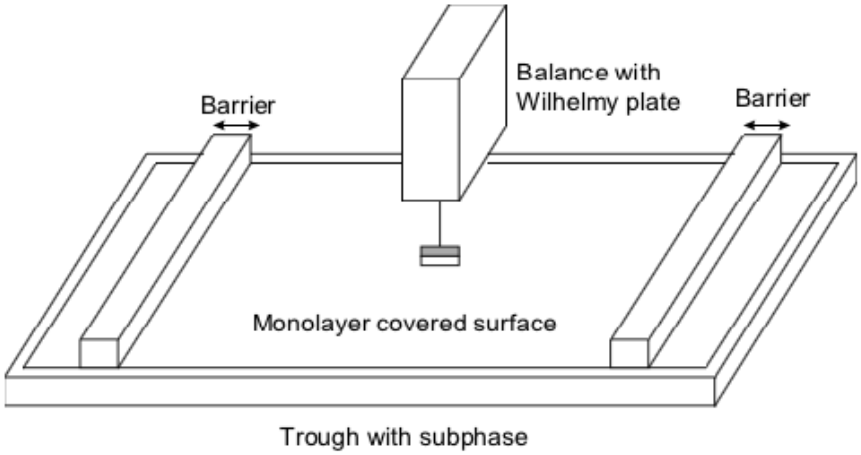

Figure 2.6. A schematic image of components of Langmuir trough. There are two barriers, a trough, and a balance with a Wilhelmy plate. The cleaned trough is filled with a subphase, which can be pure water or any kinds of suitable subphase. When organic molecules are transferred on the subpahse, the balance with a Wilhelmy plate placed over the trough measure the change of surface pressure during the experiment. The movement of barriers between the edge and the center of the trough controls the area covered with the molecules on the subphase. This figure was referred from KSVmini Manual.

2.4.1.1 Surface pressure measuring system

The system is composed of a Langmuir balance and a Wilhelmy plate. The balance with the Wilhelmy plate collects and sends the surface pressure data to software for controlling the surface pressure during the experiment. The Wilhelmy plate made of thin platinum or filter paper can be used. The immersed Whilhelmy plate and its physical dimension is displayed in Figure 2.7.

The surface pressure is calculated by the difference between γ, the surface tension with Langmuir film and the surface tension without Langmuir film γ_0 like Equation 2.1 below.

$$\Pi = \gamma - \gamma_0 \tag{2.1}$$

The net force acting on the plate is the sum of the downward forces that are the gravity and surface tension and the upward force buoyancy due to the submerged part. It is given by Equation 2.2.

$$F = \rho_{\mathrm{p}} g l_{\mathrm{p}} w_{\mathrm{p}} t_{\mathrm{p}} + 2\gamma(t_{\mathrm{p}} w_{\mathrm{p}})(cos\theta) - \rho_{\mathrm{l}} g h_{\mathrm{l}} \tag{2.2}$$

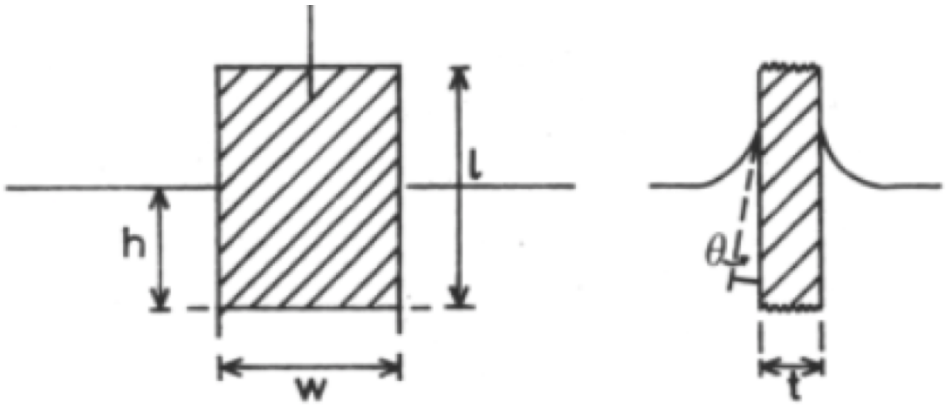

Figure 2.7. A schematic image of a Wilhelmy plate partially immersed in a subphase. The net force on the Wilhelmy plate is the sum of the gravity, the surface tension, and buoyancy. The amount of each force can be calculated using the data of the physical dimension of the plate. This figure was referred from KSVmini Manual.

Where F is the net downward force of the plate, l_p, w_p and t_p are length, width and thickness of a plate, and ρ_p and ρ_l are density of the plate and liquid, g is gravitational constant, h_l is the submerged length, γ is the liquid surface tension, θ is the contact angle of liquid on the plate.

When two barriers move to the center of the trough, the density of molecules of the monolayer becomes dense. Condensed monolayer decreases the surface tension of subphase, and this is measured by the balance recording the change of the force F on the wilhelmy plate. The surface pressure is obtained continuously from calculating the difference between the force F without a monolayer and with a monolayer. It is shown by Equation 2.3.

$$\Pi = -\Delta\gamma = -[\Delta F/2(t_\mathrm{p} + w_\mathrm{p})] = -\Delta F/2w_\mathrm{p}, if w_\mathrm{p} >> t_\mathrm{p} \qquad (2.3)$$

2.4.1.2 Film area control system

The area covered by a monolayer is controlled by two moving surface barriers. The barriers are made of hydrophilic Delrin, which prevent the monolayer on the area between the barriers from transferring to the area between the side edges of the trough and the barriers below the barriers. Their operation is controlled by parameters such as the zero position of barrier and barrier speed that were defined by the user in the KSV software. The mean molecular area is measured during the compression.

2.4.1.3 Trough

The trough is usually coated with Teflon to block unintended outflow of the subphase over the edges. Both the trough with or without a dipping well

can be used depending on the main purpose of experiment. A base plate connected to a thermostat is mounted on the bottom of the trough to control the temperature of the subphase. The thermometer can be inserted into the hole of the thermometer holder attached to the middle of the front edge of the trough.

2.4.1.4 Deposition system

The dipper is controlled by the software for unsupervised and automatic film deposition. By the help of the KSV software, a user is able to control deposition parameters such as the zero position of the substrate, deposition speed, deposition cycles, and dwell times. Two different sample holders for vertical and horizontal depositions are given by the manufacturer.

2.4.1.5 Surface pressure-area isotherms

Most of Langmuir films are created by spreading amphiphilic molecules on the surface of subphase, which have hydrophilic head groups and hydrophobic tail groups. During the compression of the barriers, the change of surface pressure is continuously measured as a function of the area occupied by molecules, while the temperature of the subphase is controlled constantly. The plot called a surface pressure-area isotherm is relevant to study because the different types of molecules draw its own unique surface pressure-area isotherm due to the properties of amphiphilic molecules and subphase. Figure 2.8 shows a schematic plot of surface pressure-area isotherm on the left-hand side and phases of Langmuir film on the right-hand side. [41]

When the amphiphilic molecules are placed on the water, the monolayer acts like a gas phase (G) first. After compression of barriers, the phase changes to the liquid-expanded phase (LE) or the liquid condensed phase (LC). The backbone chains of molecules in the liquid condensed phase are much organized than gas phase because of their ordered formation stabilized by van der Waals interactions. The last phase is the solid phase (S) and this is composed of highly packed molecules of a monolayer. After obtaining the solid phase, the extra compression leads to the collapse of formation of the monolayer that is observed a sharp decrease of surface pressure. [41]

2.4.1.6 Langmuir deposition methods

Langmuir deposition is divided into two categories such as Langmuir-Blodgett (LB) and Langmuir-Schaefer (LS) by setting a solid substrate. They are described in Figure 2.9.

LB technique submerges the substrate perpendicular to the surface of a subphase. The film created by LB method is called LB film. In contrast to LB technique, LS technique dips the substrate horizontal to the surface of the subphase. Both techniques can fabricate multiple thin films on the substrate by repeating their process.

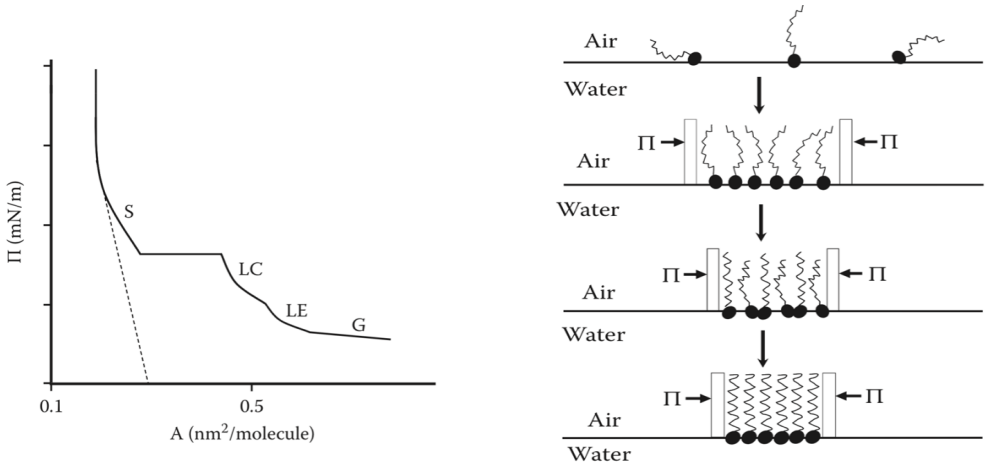

(a) A surface pressure-Area isotherm (b) Different phases of Langmuir film

Figure 2.8. Schematic images of surface pressure-area isotherm and Langmuir film. (a) Isotherm of a Langmuir film made of amphiphilic molecules consists of several phases from gas, liquid, solid, and their intermediate phase. G, LE, LC, and S mean 2-D gas, liquid-expanded, Liquid-condensed, solid phase, respectively (b) The arrangement of a Langmuir film increases as the barriers move close to the center of trough until the Langmuir film collapse. Each of phase from gas to solid on the left-hand side corresponds to each of the schematic illustration from the top to the bottom on the right-hand side. This figure was referred from the book 'Understanding nanomaterials'. [41]

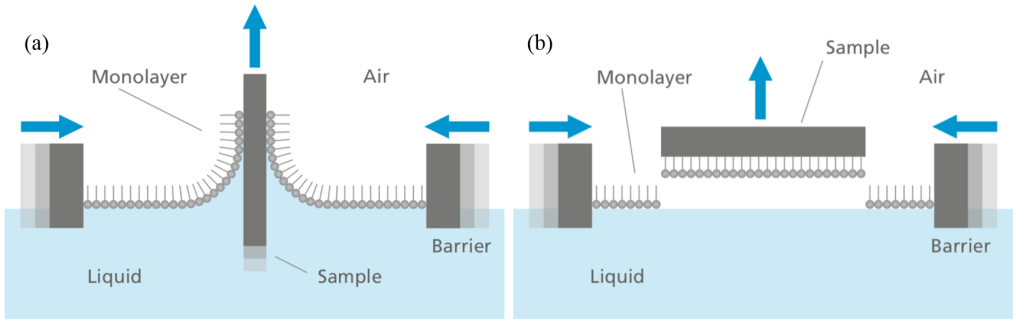

Figure 2.9. Schematic images of Langmuir-Blodgett (LB) and Langmuir-Schaefer (LS) methods. (a) A substrate erected perpendicular to the surface of the subphase is used in LB deposition. (b) A substrate lying horizontally to the surface of the subphase is used in LS deposition. This figure was referred from the webpage 'https://www.biolinscientific.com/measurements/langmuir-and-langmuir-blodgett'.

2.4.2 Recent studies of Langmuir deposition

2.4.2.1 Temperature of subphase

There are factors affecting the result of surface pressure isotherm in the Langmuir trough experiment. The temperature of subphase is one of the factors affecting the phase of Langmuir film. The thermal energy of the amphiphilic molecules of the Langmuir film is directly controlled by the temperature of subphase. So it is natural to think more thermal motions of the molecules leads to less condensed film, which gives rise to the increase of the surface pressure. The length of hydrocarbon chain of the molecules has a similar effect as well because van der Waals force acting between the molecules is affected by the length of the chain length so that the decreased length leads to a less condensed structure of the film. [56]

Dhanabalan et al. investigated the Langmuir film and Langmuir-Blodgett films of the methacrylate derivative of Disperse Red-13 molecules. [57] In the paper, they reported the opposite observation about the effect of subphase temperature to the isotherm compared to the normal effect of temperature. They stated that at 25 mN/m, increasing temperature from 8 to 33 °C leaded to a decrease of surface pressure from around 18 to 4 mN/m. In addition, the same amount of temperature change resulted in less mean molecular area from around 18 to 12.6 $Å^2$ in the solid region at 25 mN/m. They explained the reason for the opposite phenomenon of the change of rigidity/flexibility of the polymer chains that polymer chains may become more flexible with increased temperature so that it could attain a condensed phase in a smaller mean molecular area. [57]

2.4.2.2 Compression rate

Another relevant parameter of isotherm is barrier speed that can be the same as compression rate of Langmuir film. The research group mentioned in the previous section had shown the influence of compression rate on isotherm at constant pH and temperature of subphase in Figure 2.10 (a). [57] They found that collapse of monolayer took place at around 64 mN/m when the barriers moved with a high speed at 100 mm/min. The collapse pressure dropped to about 37 mN/m when the barrier moved with a low speed at 0.5 mm/min

The authors explained that this result was based on the rigidity of their molecules that the more speed of barrier applied, the less time allowed for the molecules to become arranged in equilibrium. They also added that the effect of compression rate will be different to that of simple amphiphilic molecules. [57] The same effect of compression rate observed by Rubinger et al. [58] They achieved surface pressure-area isotherms of PAN film at 22.8 °C with three different compression rates. With their results, they explained with the same idea mentioned previously that slower speed of the barriers led to more possibilities for better molecular arrangement for macro molecules as well as lower collapse pressure.

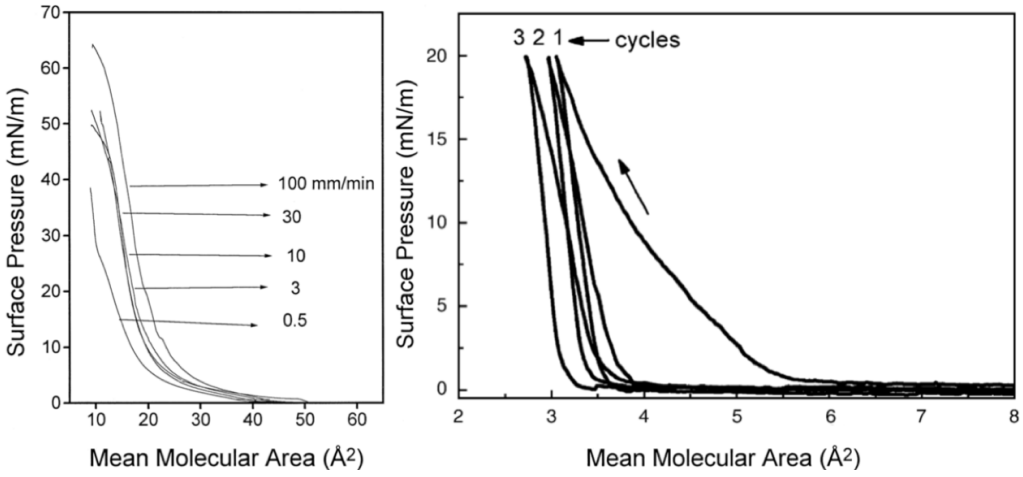

Figure 2.10. (a) Surface pressure–mean molecular area isotherms of HPDR13. The change of speed of barrier in the normal range between 3 and 30 mm/min has an insignificant impact to the surface pressure of the collapse of the Langmuir film of HPDR13. The extreme cases of the speed of barrier at 0.5 or 100 mm/min decrease or increases the collapse pressure. This figure was referred from an article by Dhanabalan et al. [57] (b) Surface pressure–mean molecular area isotherms of Langmuir PAN film at 22°C. Repetitive compression cycles draw different isotherms due to the strong interaction between molecules on the Langmuir film. This figure has been was referred from an article by Rubinger et al.. [58]

2.4.2.3 Type of the molecules

The type of the molecules influences the result of the isotherm. Rubinger et al. also commented that it could have a single Langmuir film or Langmuir-Blodgett film consisting of aggregated molecules for some materials. For example, a molecule that has a hydrogen bond can have aggregated form with adjacent molecules. [59, 60] The effect of the type of the molecules can be shown on the isotherms with a few cycles of compression-decompression of the barrier in Figure 2.10 (b). Molecules that have complex shapes are not able to display reversibility due to the aggregation caused by strong intermolecular interactions between the molecules during the compression. A certain amount of energy is needed to break the aggregations into each molecule.

2.5 UV-Vis spectrometry

2.5.1 Relationship between color and pi conjugation

It is known that the color of a certain material is determined by its own location of absorption wavelength. When a beam of white light, a mixture of red, green, and blue lights, is reflected from a material, the material absorbs a certain range of wavelength so that the observer can see the complementary color. For example, people recognize the color of beta carotene is orange due to its absorption range starting from 400 to 500 nm, which is green and blue color range. It has been reported that the absorption range of indigo lies on 540 nm (red color area) in gas phase and 588 nm (violet color area) in tetracholromethane, 606 nm in a polar solvent. [61, 62]

Several theoretical and experimental studies revealed the relationship between the absorption of the wavelength and the degree of pi-conjugated system. [63–65] These studies stated that bathochromic shift or red shift is driven by increasing the size of pi-conjugated system. They explained further that increasing degrees of pi conjugation leads to the decreasing of the energy gap between highest occupied molecular orbital (HOMO) and lowest unoccupied molecular orbital (LUMO) so that electrons in organic molecules with enough pi-conjugation can be excited easily by a longer wavelength.

It is found that the degree of bathochromic shift is stronger when indigo is in a solid film state than in solution. The reason for this is explained by the fact that indigo molecules in the film aggregate with its neighbor molecules by hydrogen bond, and lower the energy level of LUMO resulting in the decrease of the gap between HOMO and LUMO. [66, 67] The maximum absorbance of indigo in different states was reported by several reports that crystalline and amorphous indigo showed max absorbance at 680 nm, 640 nm, respectively. [68] The maximum absorbance of highly-crystalline indigo film was measured at around 700 nm. [69]

2.5.2 Recent studies of indigo by UV-Vis spectrometry

It was reported by the review paper that the absorbance peak of indigo solution took place at around 600 nm. [70, 71] Irimia-Vladu et al. reported the UV-Vis result of indigo film created by evaporation in 2011 that the absorption band of indigo thin films, laid in 450-730 nm, was red-shifted by around 100 nm from the absorption band of indigo in solution. [19] According to other articles about indigo, the absorption shift from 50 to 120 nm was observed bathochromically when the state of indigo and tyrian purple changes from a solution to a solid film. [11, 70]

2.6 Atomic force microscopy

The characterization of atomic force microscopy (AFM) is able to achieve the topography of films deposited on the substrates. AFM allows users to attain relevant information like general topography, surface roughness, size of an aggregate, and surface coverage. Two different types of articles containing AFM results were reviewed. One type is about indigo used for semiconducting film, and the other type is about organic film deposited by Langmuir deposition.

2.6.1 Indigo derivatives deposited for semiconducting film

Dharmapurikar et al., the same report referred in Section 2.2.4, characterized thin film by AFM. [10] From the images of AFM in Figure 2.11 (a), they explained that the reason for the good charge transport of poly(reg- iInd-DT) film was due to the well linked structure of nano fibers. The other films showed less connected topography or topography with some pinholes.

A study conducted by Irimia-Vladu et al., previously covered in Section 2.2.4, showed the AFM result in Figure 2.11 (b) that the size of the grains of both indigo derivatives lay in between 250 and 300 nm. [19]

Głowacki et al. explained the relationship between charge mobility and grain size in the paper published in 2013. [72] From the AFM characterization in Figure 2.11 (c), it was observed that the grain size of quinacridone films is in the range of 100 to 200 nm, which is much smaller than that of epindolidione films lying in the range of 400 to 1000 nm. Since the smaller size of quinacridone grain leaded to the increase in the number of grain boundaries so the charge mobility of quinacridone films might be less effective than that of epindolidione films.

Pitayatanakul et al. reported the result of AFM in the same report mentioned in Section 2.2.4. [21] that the indigo derivative film on a passive tetratetracontane (TTC, $C_{44}H_{90}$) layer showed highly crystalline domains like in Figure 2.11 (d). They added that TTC passive layer enhanced the crystal structure of the film.

Bonacchi et al. discussed about the AFM images of isoindigo- based conjugated polymer (IIDDT-C3) displayed in Figure 2.11 (e) that the nanofibrils of isoindigo-based polymer laid in vertically to the direction of barrier movement of Langmuir trough. [22] The measured width and length of the nanofibrils were 30 nm and 1 μm, respectively.

2.6.2 Organic films deposited by Langmuir deposition.

In 2003, Bertoncello et al. produced poly[3-30(vinylcarbazole)] (PVK) films deposited on several types of substrates by Langmuir-Schaefer (LS) deposition to investigate the photoelectrochemical properties of LS film. [73] They investi-

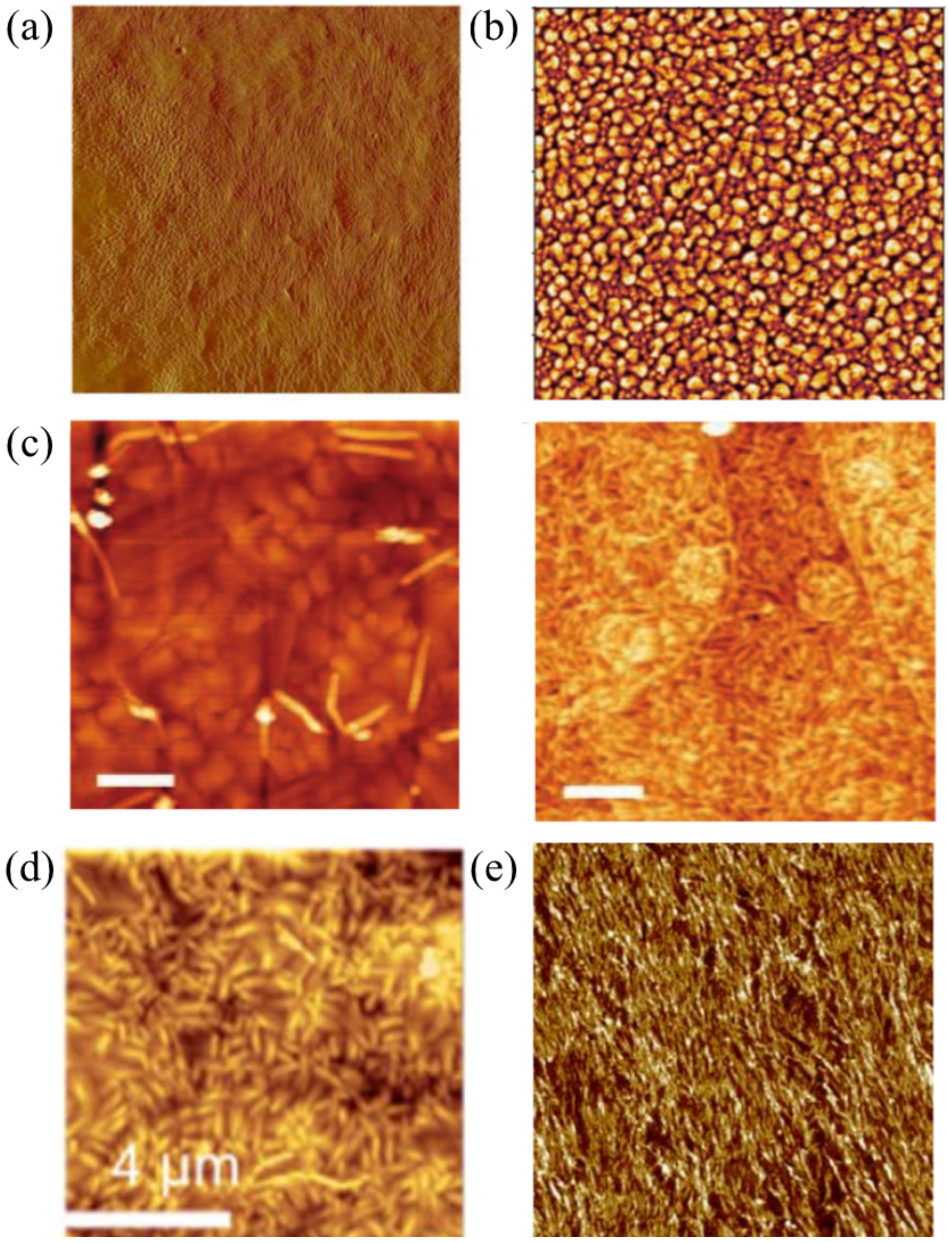

Figure 2.11. AFM images of thin films (a) Thin film of poly(reg-iInd-DT) molecules that well connected nano fibers leads to the charge mobility at $1x10^{-2}$ cm^2/Vs. [10] (b) Thin film of indigo molecules consisting of grains in the island formation shows the mobility at $1x10^{-2}$ cm^2/Vs. [19] (c) Epindolidione on the left-hand side and quinacridone on the right-hand side. The smaller number of grain boundaries of epindolidione film due to the larger grain size than quinacridone results in better charge mobility at 1.5 cm^2/Vs. [72] (d) Thin film of 5,50-diphenylindigo displayed 0.85 cm^2/Vs. [21] (e) The thin film of IIDDT-C3 polymer. The enhanced packing and low defect of film leads to a good charge mobility at 1 cm^2/Vs. [22]

gated the morphology of five layers of a PVK LS film with and without iodine doping on the silicon substrates shown in Figure 2.12 (a) and (b). It was found that the both doped and undoped PVK LS films covered the entire surface. With 0.7 μm x 0.7 μm images, the average diameters of grain of doped and undoped samples were found as about 40 nm, 50 to 100 nm, respectively. The thickness of films was measured to be about 28 nm, 5.6 nm per layer, using a scratch part made for this purpose.

In 2006, Rubinger et al. created Langmuir–Blodgett and Langmuir–Schaefer films with poly (5-amino-1-naphthol) (PAN) on hydrophilic silicon substrates. [58] In Figure 2.12 (c), the surface was partially covered by PAN film, and its coverage was 40 %. The surface roughness was 2.5 nm. Disordered agglomerates were found, and their height were about 5 nm. In contrast, LS-Pan film created by semi-dry process in Figure 2.12 (d) that no contact of the subphase showed the high quality of homogeneous and smooth film. The film covered the surface of sample completely and its roughness was 1 nm. The thickness of the film was measured to be 5 nm. They accounted for the difference between predicted values and observed values by means of LB and LS monolayers composed of aggregated molecules based on hydrogen bonding between neighbors. With respect to low coverage of LB film, they further explained about low coverage of LB film that it is common for non-amphiphilic molecules for LB films. This phenomenon happens due to aggregated molecules created from the rearrangement of molecules during the deposition if the molecules have a low molecular weight. If the molecules have a high molecular weight, desorption due to the complex forces happens on the rigid molecules during the deposition.

In 2013, Sizov et al. doped the monolayer of oligothiophene molecules on n-type Si substrates by Langmuir-Blodgett (LB) method. [74] From Figure 2.12 (e), they found that the surface coverage was higher than 90 %, and the thickness of the layer was about 3.5 nm, which is almost similar to the length of the quinquethiophene- based molecule. They accounted for lighter areas in AFM image as a bilayer domain due to dimerization of the quinquethiophene-based molecules.

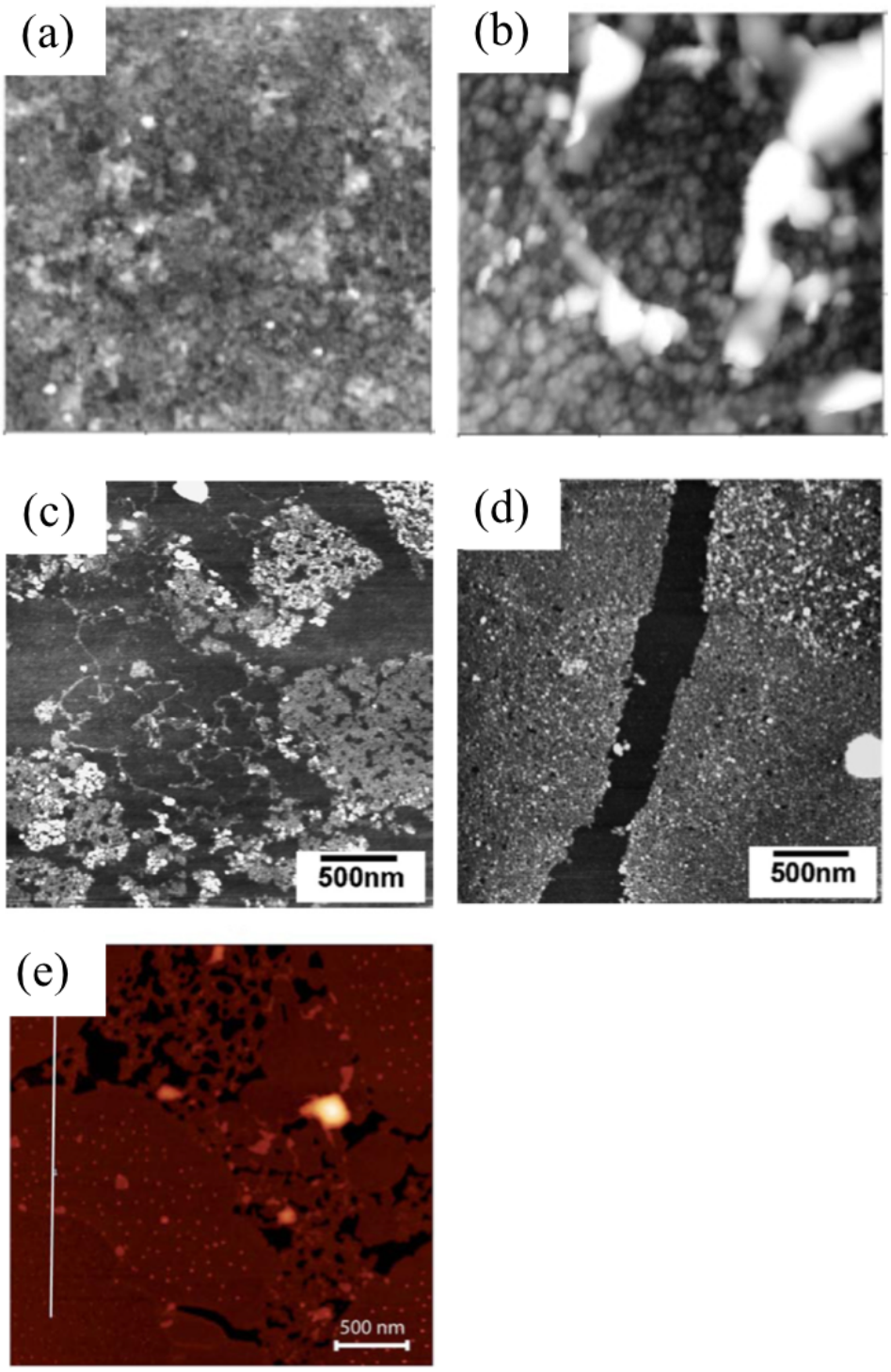

Figure 2.12. AFM images of thin films of other organic molecules by Langmuir method (a) Five layers PVK LS films without I2 doped. [73] (b) Five layers PVK LS films with I2 doped. [73] (c) Langmuir-Blodgett-PAN film. (d) Langmuir-Schaefer-PAN film. [58] (e) Oligothiophene-based film. [74]

Chapter 3

Experimental part

3.1 Chemicals and materials

All the chemicals used in the experiment were obtained from Sigma-Aldrich/Merck.

- Indigo dye, $C_{16}H_{10}N_2O_2$, CAS Number 482-89-3
- Trichloro(octadecyl)silane, $CH_3(CH_2)_{17}SiCl_3$, CAS Number 112-04-9
- Bicylohexyl (BCH), $C_6H_{11}C_6H_{11}$, CAS Number 92-51-3
- Carbon tetrachloride, CCl_4, CAS Number: 56-23-5
- Chloroform, $CHCl_3$, CAS Number: 67-66-3
- Milli-Q, 18.2 MΩcm at 25 °C
- Glass substrates
- SiO_2 substrates

3.2 Preparation of indigo solution

3.2.1 Dissolving indigo in chloroform

According to the article, the maximum concentration of indigo dye in chloroform solvent is about 100 μM. [71] The mass of indigo for maximum concentration of 100 mL is calculated below.

- Maximum concentration of indigo dye : 100 μM = 100 $\times$ 10^{-6} mol/L
- Molar mass of indigo : 252.27 g/mol
- The mass of indigo for maximum concentration of 100 mL (g/mL): 100 $\times$ 10^{-6} mol/L $\times$ 252.27 g/mol $\times$ 10^{-3} $\times$ 10^{2} = 0.0025227 g $\approx$ 0.0025 g

The indigo solution for deposition was prepared by following three procedures below. First, the amount of indigo dye was measured on a balance that has four significant figures after the decimal point. A clean empty beaker was placed on the balance, and then the balance was zeroed. Indigo powder was carefully transferred into the beaker to get as close as possible the amount of 2.5 mg.

Second, about 15 mL of pure chloroform was transferred to the beaker containing 2.5 mg of indigo dye. The beaker was tilted and rotated carefully a couple of times so that the chloroform solvent could touch the lateral side of the beaker in order to avoid undissolved indigo powder remaining in it. The solution in the beaker was poured into a 50 ml volumetric flask. These procedures were repeated three times to transfer all the indigo powder clearly from the beaker into the volumetric flask. Some amounts of chloroform were poured into the flask to fill the exact amount of 50 mL. The flask was capped and rotated for three minutes by hand to dissolve the indigo powder. Following this, the 50 mL of indigo solution was transferred slowly into a 100 mL borosilicate glass bottle. Pure chloroform was poured into the sample flask to dissolve indigo powder that had not been previously transferred. When the solution filled 50 mL in the same flask, it was poured into the same borosilicate glass bottle to fit 100 mL.

Third, the solution in the bottle was stirred by a magnetic stirrer for about two days at room temperature until the undissolved particles disappeared in the solution. The bottle was capped and stored in a fume hood at room temperature.

Two solutions with different concentrations were made, 0.022 mg/mL and 0.026 mg/mL of solutions, respectively. The first one was used for indigo deposition. The second one was used so as to be measured by UV-Vis as a reference of the maximum concentration.

3.3 Pretreatment of substrates

3.3.1 Creation of SAM layers on the substrates

A SAM layer was created for two purposes. One was to produce an insulating layer to simulate a general OFET structure. The other was that a SAM layer allow to enhance both the adhesion and crystalline structure of an organic film on the SAM layer. Sample substrates were cleaned before starting silanization. First, samples were put into a beaker filled with ethanol as an initial cleaning solvent. The beaker was placed and cleaned by an ultrasonic bath for ten minutes. After that, only the ethanol in the beaker was removed, and the beaker was filled with Milli-Q water as a second cleaning solvent and the samples were cleaned in the ultrasonic bath for another ten minutes. During the cleaning, a pair of tweezers also was cleaned in a different beaker by an ultrasonic bath. After the ultrasonic cleaning, the remaining water on the substrates were dried by nitrogen gas blower carefully. Dried substrates were placed in an UV-Ozone cleaner for ten minutes. When the process finished, the samples were moved to a Petri dish, while their ozone cleaned sides were kept in upside.

The general procedure of Lessel et al. was followed for pre-cleaning of a substrate, preparation of silane solution and coating of a silane film. [75] 5 ml of bicylohexyl (BCH) was transferred to a cleaned glass Petri dish. 0.24 μL of carbon tetrachloride CCl_4 and 0.214 μL of octadecyl-trichlorosilane were added to the solution in the dish. The dish was slowly rotated to mix the solution by hand for about one minute. Two or three of glass or SiO_2 substrates were gently put in the bottom of the dish using cleaned tweezers. The cleaned sides by UV-Ozonizer were faced the top during the whole process. The dish could be rotated additionally in case that any top sides of the substrates were not submerged. After 15 minutes of silanization, the substrates were taken out of the dish and cleaned thoroughly with chloroform from a Pasteur pipette to get rid of unattached silane molecules. The substrates were dried out completely with a nitrogen gas blower. The substrates were placed on the bottom of the dish again, and the rest of coating procedures were repeated one or two times. The silane solution was removed when the cross linking of silane molecules which looked like white flakes in the solution. a new silane solution was created and used for silanization. After that, the contact angle of each substrate was checked by a KSV contact angle meter.

3.4 Deposition of indigo

3.4.1 Deposition of indigo by Langmuir-Schaefer method

1. Cleaning and setting the trough and barriers (15 minutes)

The surface of the Langmuir trough and two barriers were cleaned with pure ethanol and then rinsed with Milli-Q water having resistivity 18.2 MΩcm at 25 °C to get rid of any residues and contaminants. During the cleaning, nitrile gloves had to be worn continually to prevent the trough and barriers from contamination by bare hands. The cleaned trough was placed on the base plate in the exact position guided by small side notches on the edge of the base plate. The barriers were inserted in the barrier holders when the holders were placed at the end of the trough. The positions of the balance and the dipper were adjusted in the middle of the trough.

2. Preparing the paper plate (30 minutes)

During the every experiment, Wilhelmy plates made of paper were used. The paper plate was placed in the Milli-Q water for at least 30 minutes before use in order to remove residues and contaminants.

3. Cleaning the surface of the subphase (15 minutes)

260 mL of Milli-Q water was poured in the cleaned trough carefully not to splash the water out of the trough. The barriers were moved to the middle of the trough until the barrier positions reached at a position of 130 mm on the monitor. The entire procedures for cleaning contained at least three rounds. Each round consisted of extracting of 0.5 mL of water at each designated point described in Figure 3.1. It was conducted by a systematic method not only to get rid of potential residues but also to adjust the height of the water level to the edge of the trough. Eight times of extracting water were performed at eight points lying on the imaginary cross sections of three vertical and horizontal lines as described in Figure 3.1, especially two times were conducted at the point of center colored in red. When the round was finished, the barriers moved back to the edge and the second round begins.

4. Hanging the plate, final cleaning and setting of the software (15 minutes)

The Wilhelmy plate was taken out of the water and hung on the hook of the balance. It was important to place one third of the plate submerged under the water and keep the position of the plate as the same in every experiment because both the position of the plate and the amount of water in the trough changes the buoyancy of the plate and affects the result of the surface pressure. The zero-balance button in the software was clicked, and the final cleaning round was performed to check that the change of the surface pressure remains less than 0.20 mN/m, which

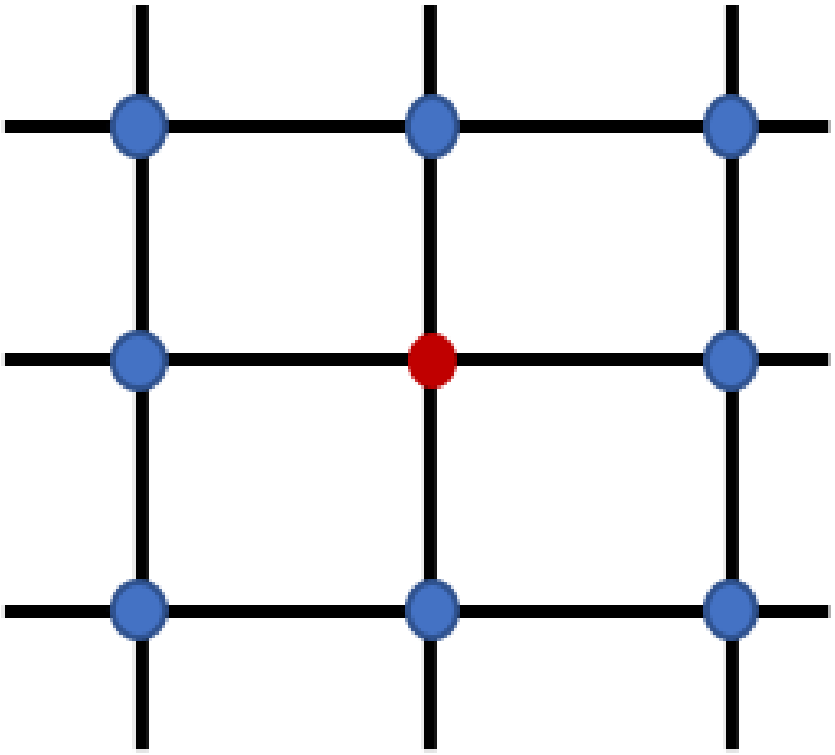

Figure 3.1. Cross sectional points lying on three imaginary vertical and horizontal lines. The micro pipette cleaned the each blue point by sucking the surface of a subphase in the trough. The red point was the spot for a Wilhelmy plate partly immersed in the subphase so that two times cleaning around the red point were conducted.

meant that the subphase was in the clean condition. One extra cleaning round could be performed usually to adjust the water level to the edge of the trough if it is needed. The barriers were opened to reach the end of the trough and the zero-balance button was clicked one more time. The settings of software such as the size of the trough and the Wilhelmy plate were checked before putting the indigo solution on top of the water.

5. Spreading indigo solution and evaporation of the solution (30 minutes)

During the process of spreading the indigo, a mask and goggles were worn all times. An 1 mL of gastight Hamilton syringe was used to spread the indigo solution on the top of the water. Indigo solution had to come out slowly and steadily from the tip of the syringe and the drops had to touch the surface of water gently. Otherwise, a falling drop could penetrate the surface of water and it would remain in the water. To get an isotherm or deposit indigo film on a substrate, 2.4 mL of indigo was spread on the water. A unit of the amount of the droplet of the indigo solution was 300 or 400 μL, and it was carefully placed around the center areas

between the center of the trough and the barriers one at a time carefully. After finishing transferring, a 30 minute wait was required to evaporate the chloroform from the surface of water.

6. Cleaning after experiment (10 minutes)

After the experiment, the water in the trough was extracted using a plastic syringe. The trough and barriers were moved to a sink and were cleaned using in the order of Milli-Q water, ethanol and Milli-Q water. The inside of the trough was brushed using a soft brush during the cleaning to get rid of residuals. When the cleaning was finished, they were moved back to the inside the box of the Langmuir instrument, and the doors of box were closed to keep the trough and barriers clean. The inside of the gas-tight syringe and the needle had to be cleaned with acetone and ethanol several times and then dried.

3.5 Instruments

Atomic force microscope (AFM). AFM was used to acquire a high-resolution image of topography of a sample surface. AFM consists of a cantilever and its tip, position-sensitive photodiodes for monitoring bending of the cantilever.

There are three different modes in AFM. These are contact, tapping, and non-contact modes. In contact mode, the tip keeps touching the sample surface during the operation. In tapping mode, the cantilever oscillates and brings the tip to touch the surface lightly. Non-contact mode is operated for avoiding tip touching the surface of a sample. Depending on which mode is used, AFM can run a destructive or non-destructive method. [41, 76]
In this experiment, the topography of indigo thin film on the SiO_2 samples was characterized in tapping mode by Bruker Multimode 8 instrument. All samples were dried and cleaned with N_2 gun before the analysis.

Ultraviolet–visible spectroscope (UV-Vis). It uses light in the range of ultraviolet and visible to check unique absorption and reflection response of samples. Absorption of light by a sample happens when pi-electrons or non-bonding electrons in the molecules are excited to a higher energy orbital by the energy of light. The spectrometer records each result and presents a graph of absorbance (A) in y-axis, wavelength (nm) in x-axis. UV-Vis is performed usually to obtain quantitative information about the samples. A sample needs to be transparent so it can be a liquid or solid type. The degree of absorbing is proportional to the concentration of the elements absorbing in the sample. It is shown by the Beer - Lambert law as below. [77]

$$A = log_{10}(I_0/I) = \varepsilon cl \tag{3.1}$$

I_0 is the initial light intensity, I is the light intensity after it passes through the sample, ε is the molar absorption coefficient, c is the concentration of the

solution, and l is the length that the light passes through. Indigo solution was characterized by UV-1800 (Shimadzu Corp.) and it was operated to analyze for indigo solution and thin films. Both characterizations were performed in the range of 200 and 800 nm. Before measuring, pure chloroform and a glass sample were used for baseline.

Optical spectroscope (OM). Optical microscopy is a one of the basic methods for checking the morphology of samples. Light reflected from the sample passes a set of lenses to amplify the image. In this experiment, A Canon optical microscope was used, which has four objective lenses from 10 to 100x. The sample checked by the optical microscope can be divided into three categories: pure SiO_2 and glass substrates, silanized SiO_2 and glass substrates, indigo films on glass and SiO_2 substrates. An internal light source from the bottom of the optical microscope was ineffective for SiO_2 sample due to its opaque property. So an external light source was used for SiO_2

Chapter 4

Results and discussion

4.1 Surface pressure-area isotherms of the Langmuir film of indigo

4.1.1 Isotherms at the same temperature

The concentration of indigo solution was fixed, and different amounts of indigo solutions from 0.15 to 2.4 mL were used to draw surface pressure - area isotherms. The result is displayed in Figure 4.1.

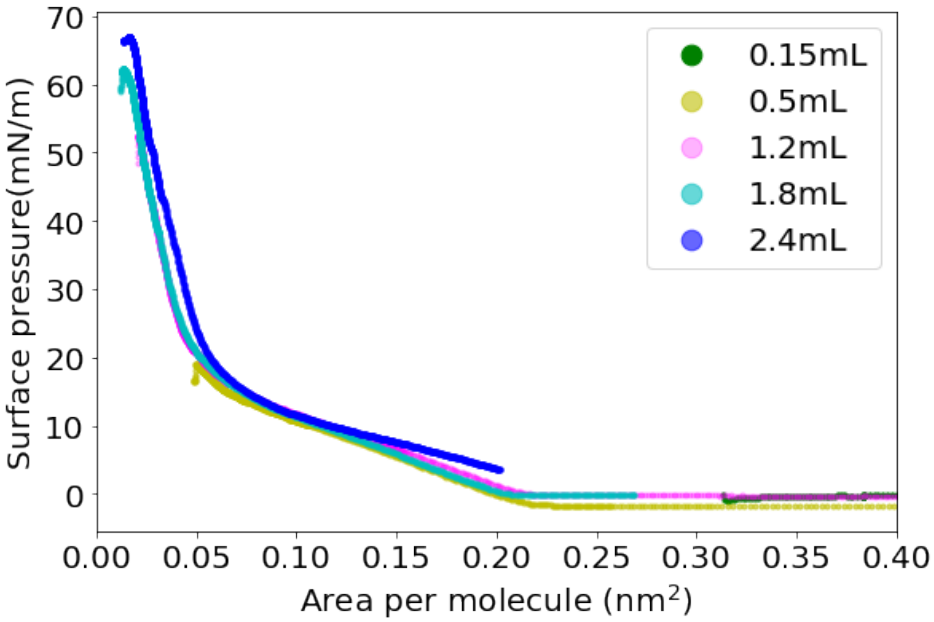

Figure 4.1. Surface-area per molecule isotherms of indigo with different amounts of solutions at 21 °C. The solution having 0.022 mg/mL of concentration was used. The speed of the barriers varied when the barrier reached to different areas of trough. The modification of the barrier speed is described in Table 4.1.

The all isotherms have similar trajectories. In addition, it is able to extrapolate zero pressure from the solutions less than 1.8 mL taking place at around 0.22 nm^2 of area per molecule. The Langmuir film of indigo collapsed at around at around 67 mN/m surface pressure in the case that 2.4 mL of the solution was used. The rest of sharp decreases happened when one of the barrier of

Table 4.1. Speed of barrier according to trough area

	Area between barriers							
Area (cm^2)	244.5 ~ 140	140 ~ 94	94 ~ 80	80 ~ 65	65 ~ 50	50 ~ 42	42 ~ 30	After 30
Barrier speed (mm/min)	30	20	10	8	6	4	2	1

Langmuir trough hit the Wilhelmy plate. The solutions could have been compressed more if the barrier had had enough space to go without touching the Wilhelmy plate. After the collapse, it was possible to observe indigo aggregates looking like a few thin hair-like on the water subphase shown in Figure 4.2.

After the barriers moved back to original positions, some of these hair-like aggregates disappeared. However, some aggregates remained on the subphase. This implies that the Langmuir film of indigo has irreversible behavior. Based on the results from UV-Vis and AFM characterization in section 4.3 and 4.4, the Langmuir film of indigo may be composed of monomers with aggregates together after at least 10 mN/m of surface pressure. This agrees with the findings made by Rubinger et al. that some materials can have a Langmuir film with aggregated molecules. The aggregates on the water subphase could be H-aggregates, which affect to attain hypsochromic absorption band, due to the limitation caused by two-dimensional space on the subphase compared to three-dimensional space in the high concentration of indigo solution. In addition, fast compression rate does not allow molecules to have time to arrange in an organized structure.

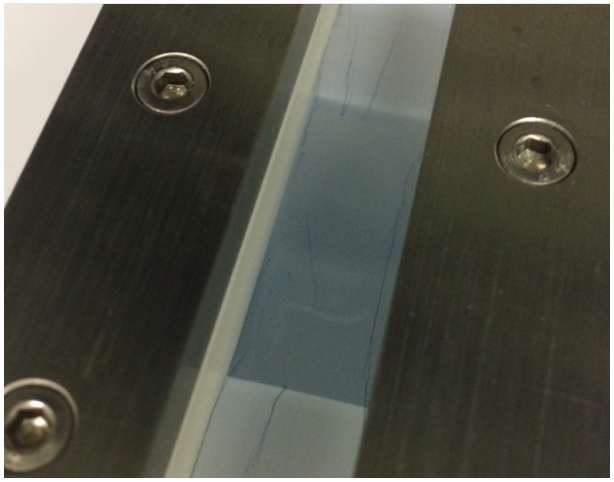

Figure 4.2. Image of indigo aggregates during the compression. The blue color lines in between two barriers are indigo aggregates.

4.1.2 Isotherms at different temperatures

As explained in section 2.4.2.1, the temperature of the subphase directly affected the shape of isotherm in Figure 4.3. First, the location of zero pressure increases from 0.22 to 0.33 nm^2 as the temperature increases from 21 to 29 °C. Second, the isotherm at 29 °C shows increased surface pressure at the same area compared to the isotherm at 21 °C until the surface pressure reached at 30 mN/m. In addition, more area is needed to get the same surface pressure compared to the isotherm at 21 °C. This agrees with the general temperature effect of Langmuir trough described in Section 2.4.2.1 that increasing the thermal motions of molecules leads to less condensed film.

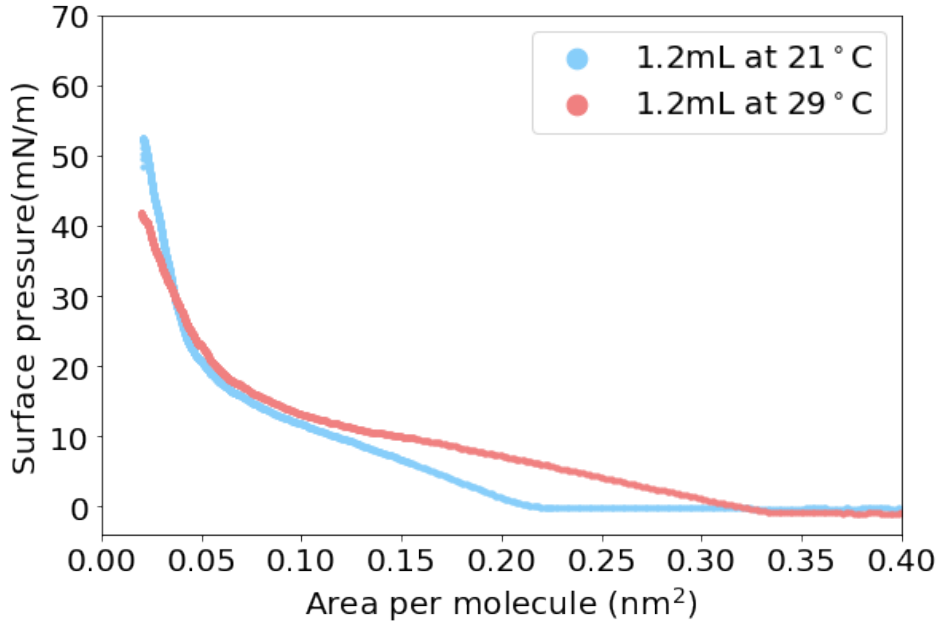

Figure 4.3. Surface - area per molecule isotherms of indigo with different temperatures at 21 °C and 29 °C. The 1.2 mL of 0.022 mg/mL of solution was used. The speed of barriers varied according to different area of the trough is described in Table 4.1.

Dhanabalan et al. explained that increasing the temperature led to more condensed film because the methacrylate derivative of Disperse Red-13 became more flexible. [57] This positive impact of flexibility of a molecule by increased temperature was not observed on the indigo film. The reason temperature having less impact on flexibility of indigo molecule could come from the simple structure of indigo molecule compared to the methacrylate derivative. Therefore, it can be thought that the no or insignificant effect of temperature on the flexibility of indigo was found in the range of temperature range between 20 and 30 °C.

4.2 Optical microscopy images of the substrates and indigo film

4.2.1 Silanized glass substrates

Since the condition of an insulating layer is able to affect the crystallinity and adhesion of a semiconducting layer above the insulating layer of an OFET, it was worth to check which parameter can influence a silane layer as the insulating layer. To make two different types of silanized glass samples, drying the sample surface with nitrogen gas before and after silanization iterations was chosen as a manipulated variable. The drying procedure applied to Lot number 1 and 2, not applied to Lot number 3 and 4. The rest parameters such as cleaning procedure, temperature during the silanization, the amount of chemicals for silane solution, the number of iterations, and silanization time were fixed as control variables. Each of the lot was created in different batch. The results of microscopy images of silanized glass in shown in Figure 4.4

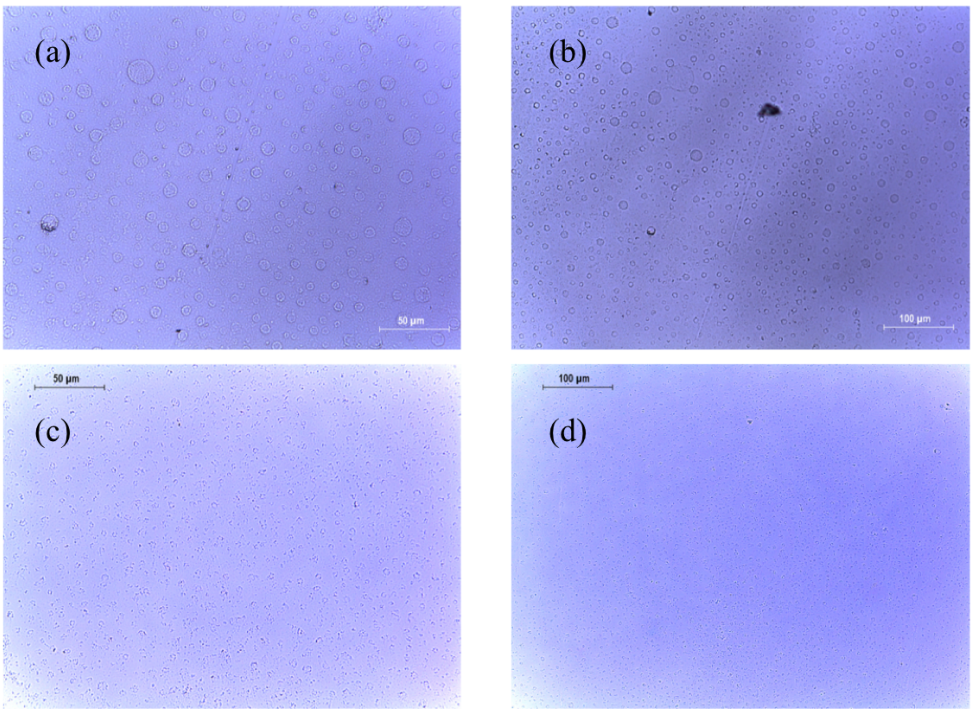

Figure 4.4. Silanized surface of glass. The top two images (a) and (b) are from Lot 1 and Lot 2, respectively. The bottom two images (c) and (d) are from Lot 3 and Lot 4, respectively. Nitrogen gas cleanings to dry the surface before and after silanization were applied to all Lot 1 and 2 samples not Lot 3 and 4. It is possible to observe that images (a) and (b) show more bigger and distinctive a globular pattern than images (c) and (d).

All samples show tiny dot patterns that average size of the dot lies in between 5 and 30 μm. It was found that there was a difference in the shape and the average size of the patterns between Lot 1, 2 and Lot 3, 4. The samples from Lot 1 and 2 have more distinctive a globular shape of the pattern, and the average size of a pattern is bigger than the samples from Lot 3 and 4.

A contact angle was chosen as a dependent variable. Two times of contact angle measurements were conducted at two different positions per sample. The average value of the two measurements was selected as a representative value for a sample. The box plot and the summary of analysis of variance (ANOVA) of the contact angles are displayed in Figure 4.5.

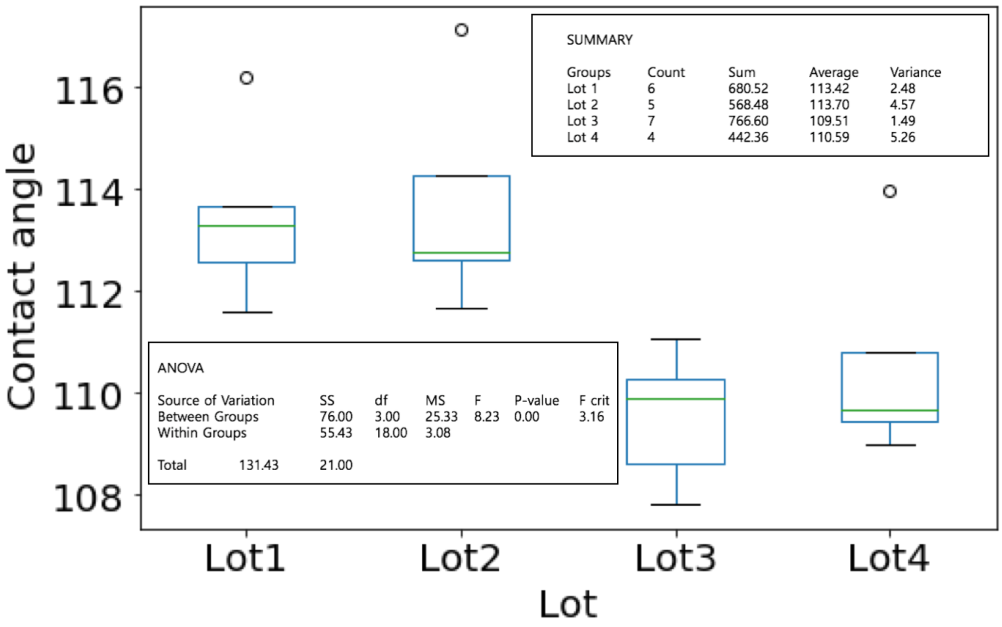

Figure 4.5. Box plot and the summary of analysis of variance (ANOVA) of contact angle data of the silanized glass samples. Lot 1 and 2 are the samples treated nitrogen gas cleaning after the silanization and Lot 3 and 4 are not treated. The box plot shows that the average contact angle of Lot 1 and 2, are higher than that of Lot 3 and 4. The Green line in each box means its median value. The top and bottom sides of each blue box means 75th percentile and 25th percentile, respectively. Whiskers from the boxes mean several possible values, and a dot out of any whisker means existance of an outlier. The top subset is the summary of the box plot, and the bottom subset is the summary of ANOVA. P-value less than 0.05 means that at least one of Lots have a different mean value than other Lots.

According to Figure 4.5, it is observed that drying the sample surface with nitrogen gas between each iteration can increase contact angle by 5 to 10 degrees based on the p-value from the ANOVA. In addition, at least two times of iterations can guarantee a contact angle around 110 degrees.

4.2.2 Indigo films on the silanized glass substrates

In Figure 4.6, it is observed that the dot pattern originated from silanization in all images after the deposition of indigo film. In order to limit the effect of the condition of silane layer, only samples from Lot 1 and 2 were used for deposition of indigo film. On top of the patterns, the blue color tends to become darker as the surface pressure and/or the number of deposition cycles increase.

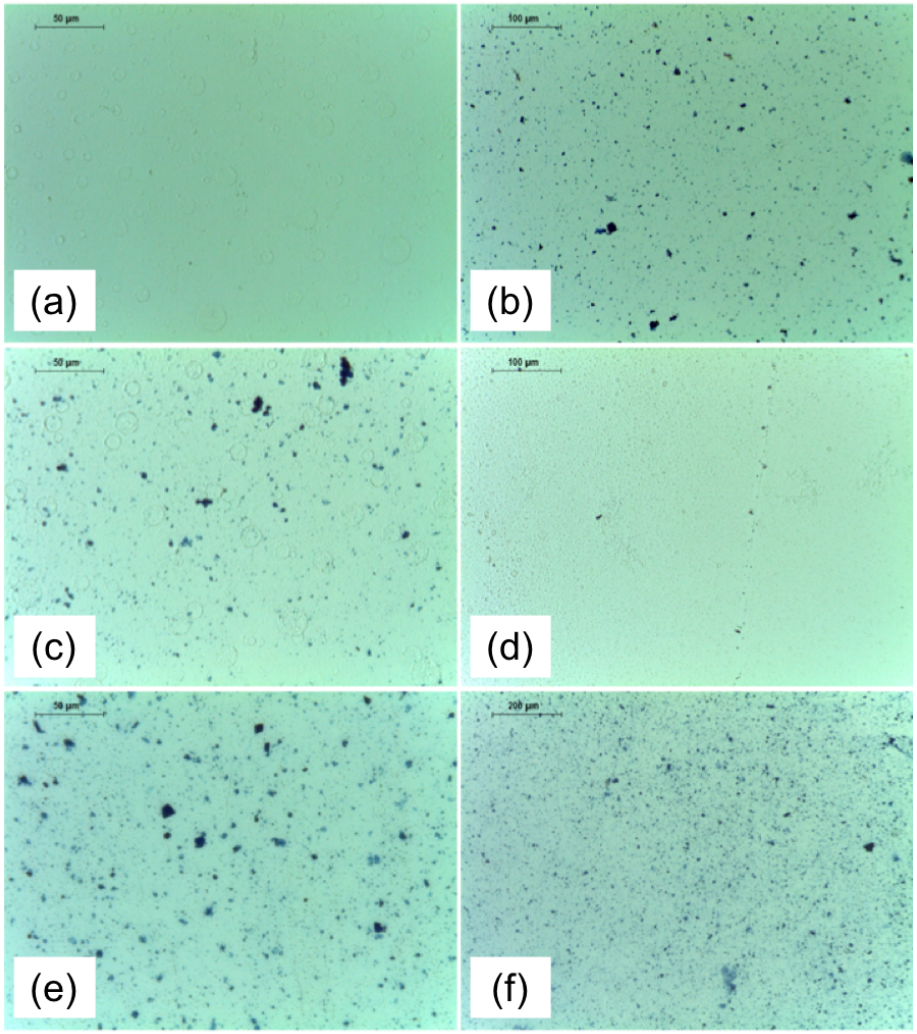

Figure 4.6. Optical microscopy images of indigo films on silanized glass. The sample were selected from Lot 1 and 2 that showed a higher contact angle than Lot 3 and 4. The images on the left-hand side were created with one deposition, the rest on the right-hand side were created with three deposition. The pairs of top, middle and bottom images were created at 20, 40, and 60 mN/m, respectively.

4.3 UV-Vis characterization

4.3.1 Results of indigo solution

UV-Vis spectroscopy was conducted to study the relationship between the concentration of indigo in chloroform and its optical properties. The original indigo solution sample was considered as having around 0.026 mg/mL concentration. Due to the limitation of the balance used to measure the mass of the indigo powder, the exact concentration of indigo might lie in between 0.026 to 0.027 mg/mL. The rest of indigo solution samples were made from the original one by diluting. The result of UV-Vis spectroscopy of different concentrations of indigo solution is shown in Figure 4.7. The summary of this UV-Vis data is organized in Figure 4.8.

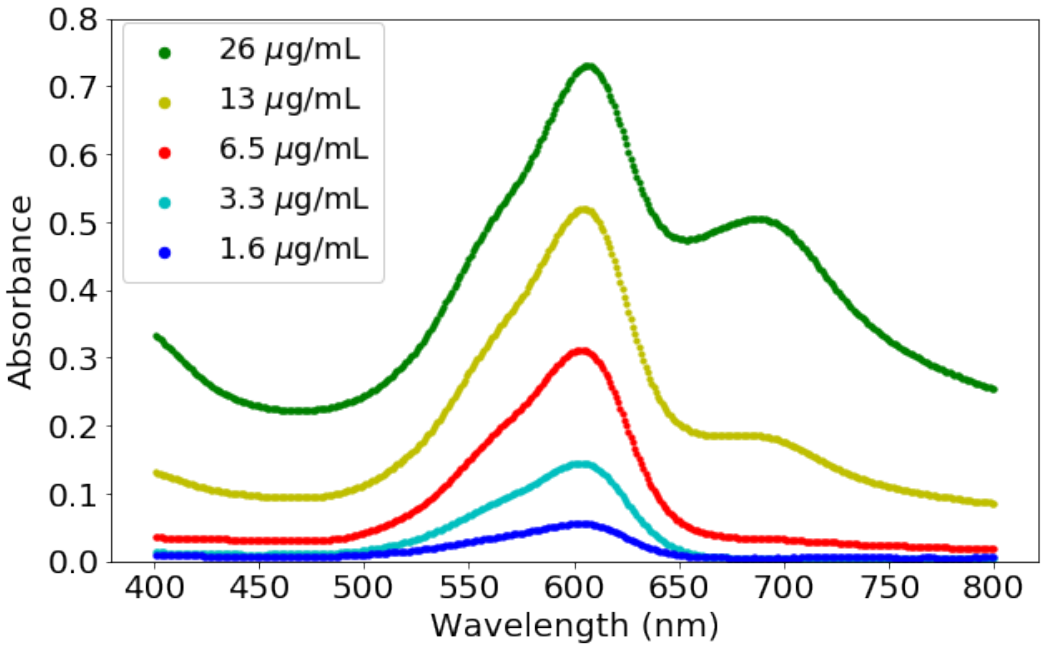

Figure 4.7. UV-Vis absorption of the indigo solution from 400 to 800 nm of wavelength. Two new absorption shoulder at around 700 nm are observed over the concentration 13 μg/mL.

All peaks of maximum absorption lie in the range of wavelength from 601 to 607 nm and this result is in accordance with the UV-Vis results reported in the papers that dealt with indigo. [67, 68, 71, 78, 79] As expected based on the Beer-Lambert law, the absorbance of a peak increases with increasing the concentration of the indigo solution. However, it does not appear the exactly proportional. According to a book about chemical analysis, there are some limitations to apply the basic concept of linearity of concentration and absorbance. [80] First, a limitation can be caused from the concentration of

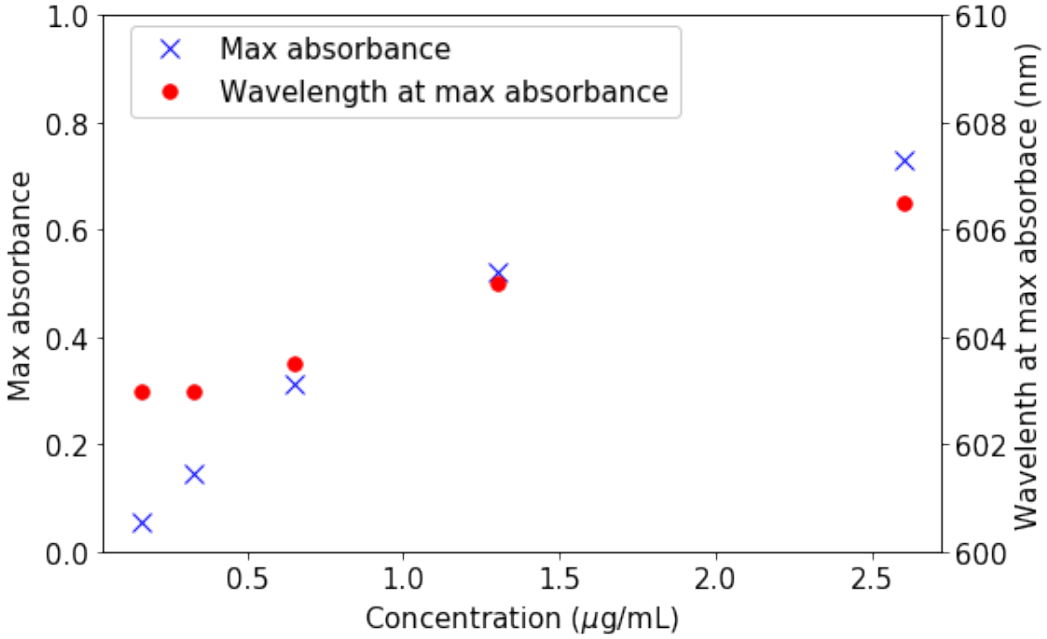

Figure 4.8. Summary of UV-Vis data of indigo solution. As the concentration of solution increases, the max absorbance increases but not proportionally and the wavelength at the max absorption peak is red-shifted.

solution. Less than 0.01 M of the concentration is allowed to avoid from an unwanted the interaction between solute molecules. Second, a further limitation can be produced by chemical deviations such as associations, dissociations, and chemical reactions between solvent and solute molecules. Finally, a limitation can come from instrumental deviations by polychromatic radiation, which means not using a monochromatic source or by stray light occurring outside of the chosen wavelength by light scattering or diffraction. [80] By considering all these constraints, the inexact proportionality could have been caused by two possibilities. One is the aggregates of indigo generated by the high concentration of solution. The other is an inaccuracy during the process of diluting the original solution.

Several studies have reported that deviations of the Beer-Lambert law could occur when the solution is not homogeneous, so it consists of different sizes of particles. [81, 82] This can give rise to the idea that a portion taken out of the bulk indigo solution had already have heterogeneous sizes of indigo particles. The results of several research reported that the emergence of a shoulder band at around 700 nm at high concentration of indigo meant the evidence of the existence of J-type aggregates, which display the bathochromically shifted bands. They noted that this phenomenon depends on the concentration of solution. [67, 78] This J-type aggregate has the face-to-face arrangement of molecules like in Figure 4.9, which was previously described in Section 2.2.2. This creation of J-type aggregates can explain more absorption of shoulder

band at around 700 nm next to the peak of maximum absorption as the concentration increases above 0.013 mg/mL.

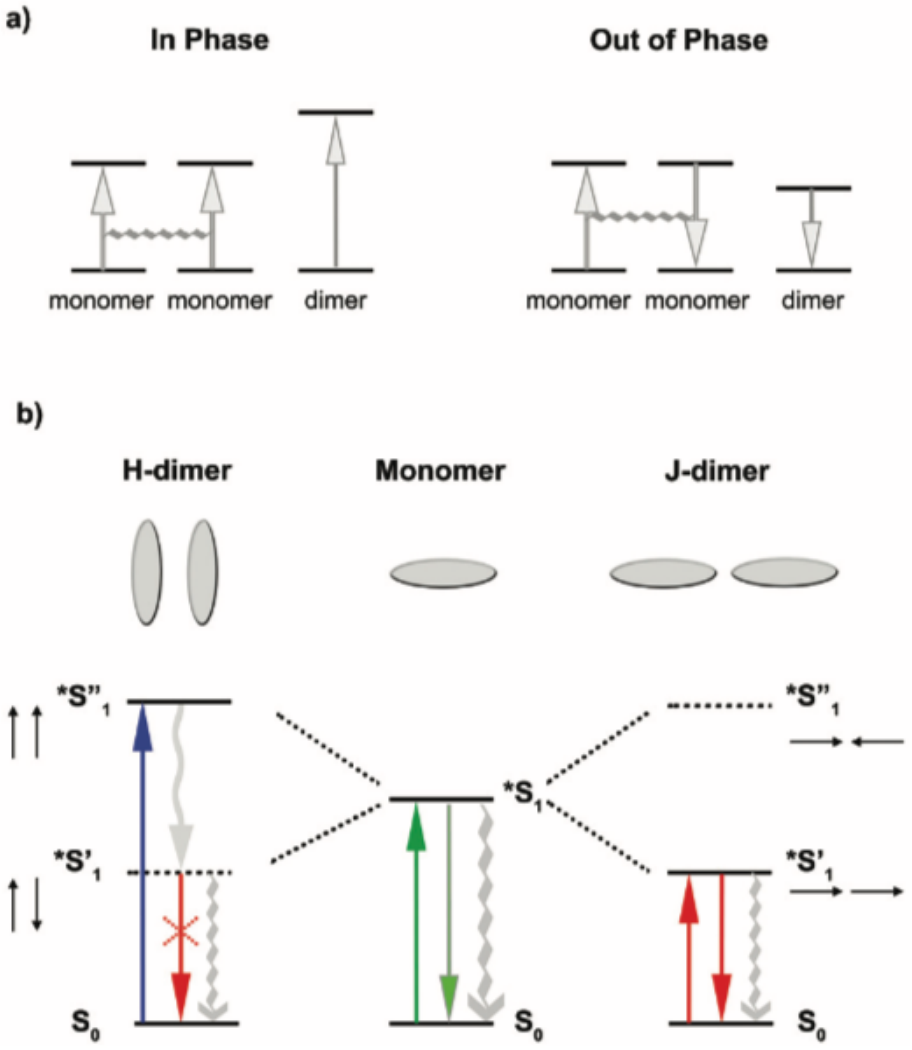

Figure 4.9. Schematic images of H-dimer and J-dimer in/out phase and their excited states. (a) The schematic images that the excited state of dimer is affected by the interaction of dipole moments of in and out of phase. (b) The top two images next to monomer image describe the molecular arrangement of the dimer. The Bottom images describe the excited and de-excited level of energy. In the case of H-dimer consisting of parallel monomers, the lowest level of energy (*S_1') is not allowed so that blue-shift of absorption band is observed. In the case of J-dimer composed of an in-line of monomers, however, the highest level of energy (*S'$_1$') is forbidden so that the absorption band is red-shifted. This picture was referred from the article 'Self-assembly of organic dyes in supramolecular aggregates'. [83]

The sufficient amount of chloroform for diluting might not have been poured or more amount or indigo solution could have been used during the diluting of 0.026 mg/mL to its half concentration, and this kept affecting the concentrations of the remaining of samples. It might be reasonable to suggest that the proportionality cannot be found in the range of concentration from 0.0016 to 0.0065 mg/mL, which does not show the shoulder peaks at around 700 nm wavelength.

The wavelength of max absorbance (λ_{max}) shows a small bathochromic shift as an increase of the concentration. This may be resulted from decreased the gap between the excited state and the ground state by less solvent.

4.3.2 Results of indigo film on glass

The result of UV-Vis spectroscopy of indigo films on the glass created at different surface pressure is shown in Figure 4.10, and the summary of this UV-Vis data is organized in Figure 4.11. In Figure 4.10, the average wavelength of max absorbance of the indigo film shows a bathochromic shift by about 70 nm compared to that of the indigo solution. Several research group observed and explained this phenomenon that pi interactions are strengthened by the effect of a hydrogen-bonded structure between indigo molecules on the substrate. [69, 84]

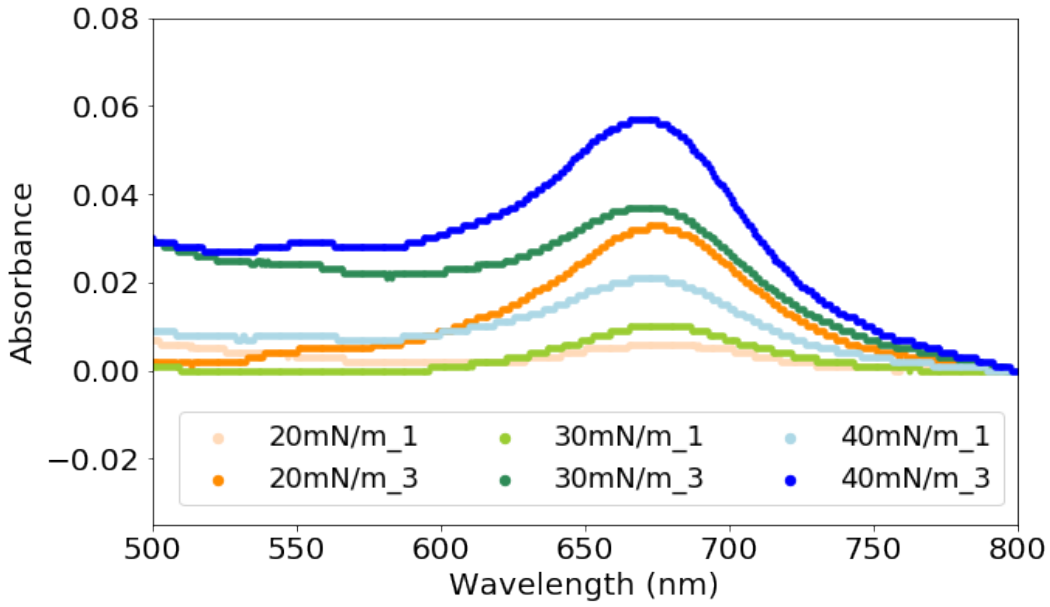

Figure 4.10. UV-Vis absorption of indigo films on the glass from 500 to 800 nm. The number of deposition cycles was written after a surface pressure. For example, the spectrum 20mN/m_1 means that the indigo film was created at 20mN/m with one deposition and 40mN/m_3 means that the indigo film was created at 30mN/m with three deposition.

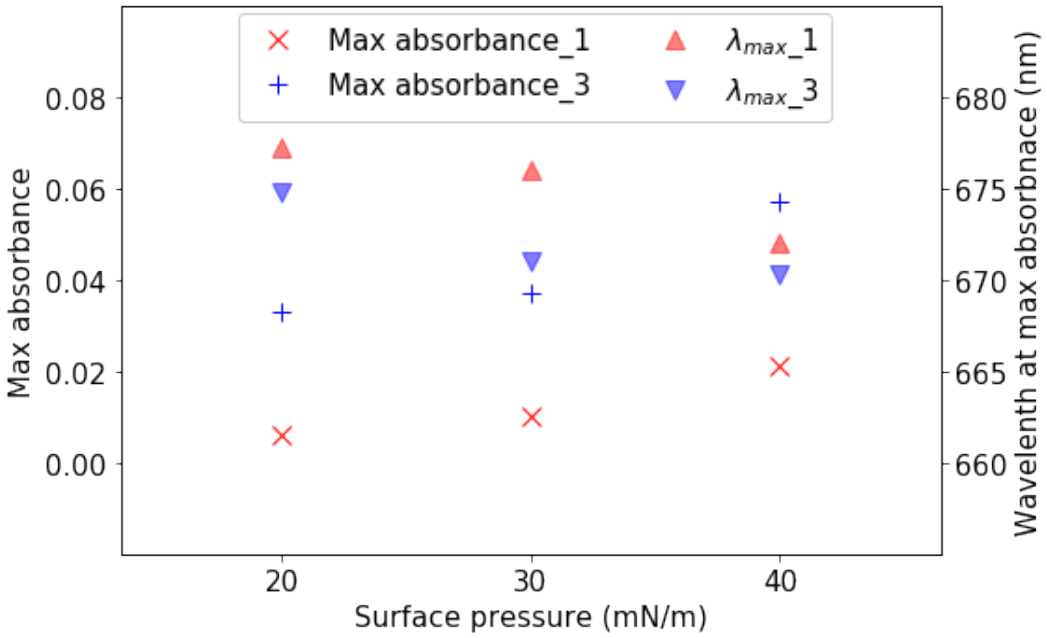

Figure 4.11. Summary of UV-Vis data of indigo films on the glass. As the surface pressure increases, the value of max absorbance increases, but the wavelength at max absorbance decreases. The wavelength at max absorbance is blue-shifted as the surface pressure increases and/or the number of deposition cycles increases.

Monahan et al. have reported that the wavelength of max absorbance ($\lambda_{\max}$) of crystalline indigo film they created was 680 nm. An amorphous indigo film was 640 nm, which means that the amorphous film has a less ordered hydrogen-bonded structure than the crystalline indigo. [68]

Several papers have reported about the actual crystal structure of solid-state indigo that each of indigo molecule is connected by four adjacent molecules with hydrogen bonds described in Figure 4.12. In addition, studies of infrared spectroscopy gave extra information about the arrangement of hydrogen bonded indigo that crystalline film has much fewer sites of free carbonyl group than amorphous film. [67, 68, 85, 86]

In Figure 4.11, the $\lambda_{\max}$ displays the hypsochromic shifts as the increase in the number of layers and/or the increase of the surface pressure. As other parameters of Langmuir trough were controlled in all experiment and no heat treatment was applied after the deposition, it could think that decreasing surface pressure has a positive effect to achieve an ordered structure. In addition, this implies that the Langmuir film of the indigo less than 20 mN/m of surface pressure could lead to a more ordered Langmuir-Schaefer film of indigo than the film created at 20 mN/m. This is an opposite tendency compared to the general tendency of Langmuir film made of amphiphilic molecules that high surface pressure before the collapse lead to a more ordered structure than

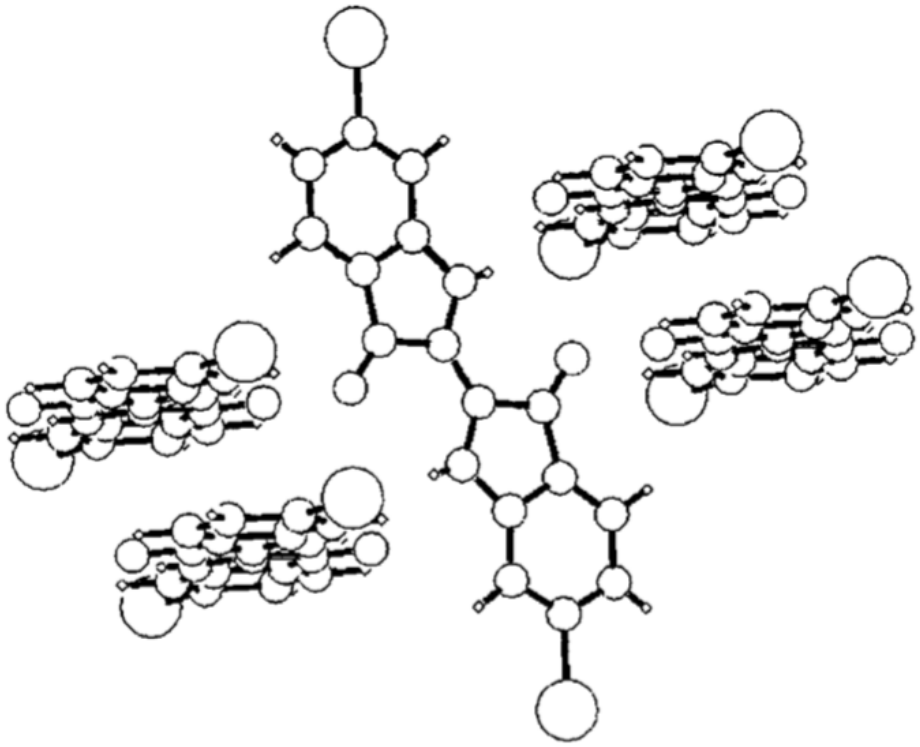

Figure 4.12. Schematic images of the structure of crystalline indigo as determined by X-ray crystallography. [86]

low surface pressure. This also lead to an idea that parameters such as the temperature of subphase, the speed of the barriers, and the idle time for rearrangement of molecules on the subphase before deposition may have strong effects to achieve the order of Langmuir and Langmuir-Schaefer films.

A research group deposited indigo derivatives by Langmuir-Schaefer method and presented general results that higher surface pressure leads to a organized structure. [22] The reason they achieved a different result even though using the same deposition method is that the molecule they used has a long hydrophobic chain, which is similar to amphiphilic molecule compared to indigo molecule. Therefore, their result followed the general tendency of Langmuir film that high surface pressure resulted in high ordered Langmuir film, and it was deposited to the substrate.

4.4 AFM characterization

All indigo films characterized by AFM were deposited on the silanized SiO_2 surfaces. The dipping speed of the Langmuir trough was fixed at 0.4 per second both up and down cycles. R_a stands for the arithmetic average of the absolute values of the profile height, and R_q stands for the root-mean-square average of the profile height. Max and Min stand for the maximum profile peak height and the minimum profile peak height, respectively. R_a and R_q of films were calculated by following expressions described in the summary report of nanoscale roughness measurement. [87] The unit of R_a, R_q, Max, and Min is nm.

$$R_{\mathrm{a}} = \frac{1}{N^2}\sum_{y=1}^{N}\sum_{x=1}^{N}|Z_{xy}| = (|Z_{11}| + |Z_{12}| + ... + |Z_{NN}|)/N^2 \tag{4.1}$$

$$R_{\mathrm{q}} = \left[\frac{1}{N^2}\sum_{y=1}^{N}\sum_{x=1}^{N}Z_{xy}^2\right]^{\frac{1}{2}} = \left[(Z_{11}^2 + Z_{12}^2 + ... + Z_{NN}^2)/N^2\right]^{\frac{1}{2}} \tag{4.2}$$

In this analysis, N is 256 due to the fact that each raw data of used AFM image consisted of 256 x 256 points of height profiles.

4.4.1 Images of SiO_2 and silanized surface

The results of AFM characterization of pure and silanzied SiO_2 surfaces are displayed in Figure 4.13. Pure SiO_2 surface showed the smoothest surface among other characterized samples. A few bright spots showing around 4nm height might have come from remained residues after the pre-cleaning process without piranha solution treatment.

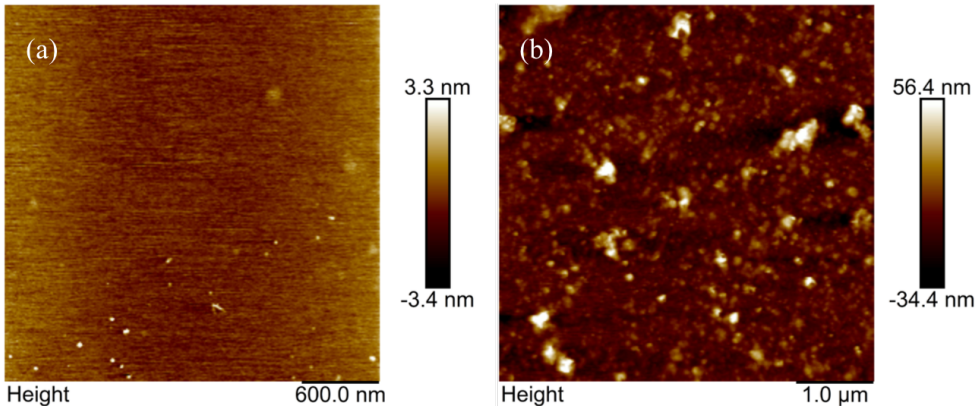

Figure 4.13. AFM images of pure and silanized SiO_2 substrates. (a) The Ra, Rq, Max and Min of pure SiO_2 substrate are 1.5, 1.7, 6.6 and -4 nm respectively (b) The Ra, Rq, Max and Min or silanized SiO_2 substrate are 7.6, 12.0, 102.0, -15.0 respectively.

It was observed that silanized surface consisted of irregular islands having a various range of heights up to 102 nm. According to the studies of silane surface, the reported height and Rq of silane monolayers created in a wet condition are about 0.1 nm and 0.6 nm, respectively. [75, 88] The measured Rq in this experiment was 12.0 nm, which is at least 20 times greater than the reported results. Based on the results by previous research, it can be analyzed that silanized surface in Figure 4.13 (b) does not have a monolayer, but layers with island aggregates like in Figure 4.14.

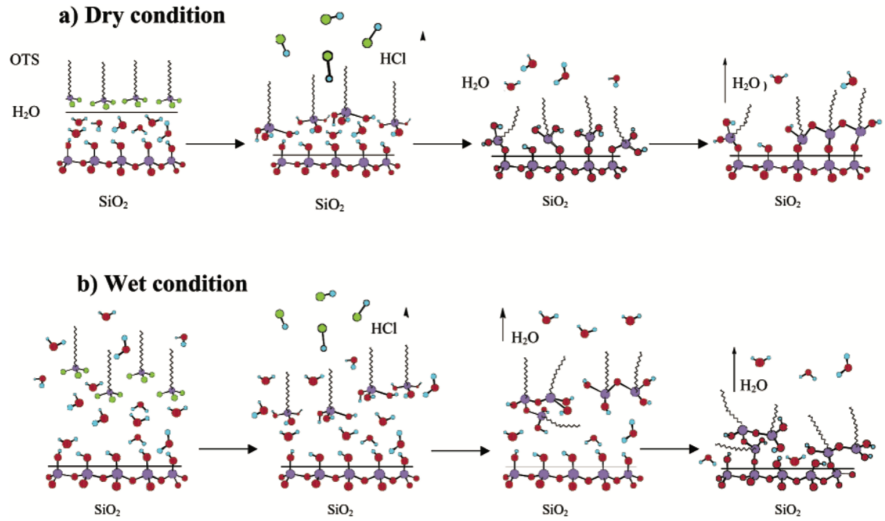

Figure 4.14. Mechanism of OTS film growth in (a) dry and (b) wet conditions. (a) In dry condition, OTS molecules attach next to OTS molecules on the surface due to the absence of secondary nucleation. The speed of nucleation is slow, but gives the smooth surface of OTS film. (b) In wet condition, hydrolysis of OTS molecules happen, and react with other OTS molecules so that aggregates of OTS are created. These aggregates may cover the surface of substrate. This figure is referred from an article "Growth of Ultrasmooth Octadecyltrichle orosilane Self-Assembled Monolayers on SiO_2 [88]

Wang et al. explained this phenomenon that secondary nucleation occurring in wet condition results in altering the thickness and roughness of silane film. [88] After each silanization process, it was observed the creation of water film originated from the ambient air in the laboratory room touching the cooled surface as a result of evaporation of chloroform used for cleaning the substrate. The added water on the silanized surface could have led to the irregular multilayer growth of silane film.

4.4.2 Thickness of indigo thin film

The thickness of indigo film was measured by comparing spots with and without indigo film created at 30 mN/m of surface pressure from the picture in Figure 4.15. The calculated thickness of indigo film was around 5 nm. This

result is similar to the thickness of indigo derivative (IIDDT-C3 polymer) monolayer(4.6 nm) created at 25 mN/m of surface pressure by Langmuir-Schaefer method. [22] This fact may imply that thickness of indigo film is close to the thickness of monolayer. However, spots having more than 10 nm of heights in Figure 4.15 could be meant that the film composed of monolayer as well as indigo aggregates.

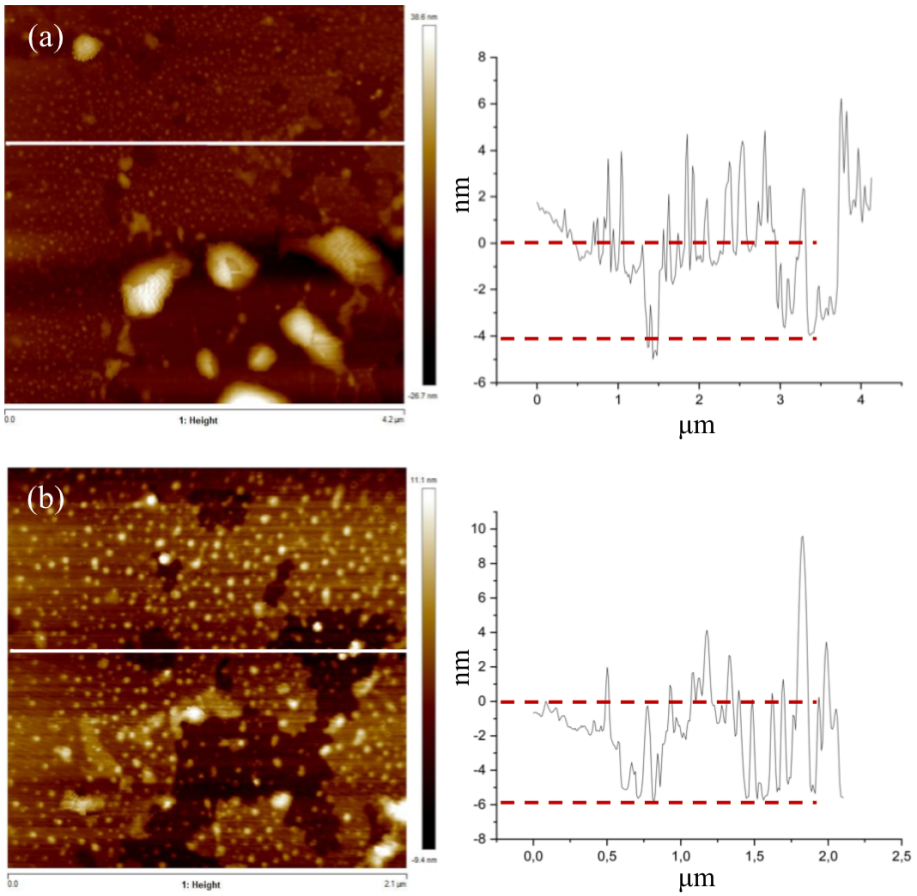

Figure 4.15. Section profiles of indigo films created at 30 mN/m. Two different areas of indigo film were characterize on the left-hand side. The z-profile of indigo film were measured by analyzing the white line on each AFM image. The thickness of indigo film is (a) 4 nm and (b) 6 nm.

4.4.3 Effect of surface pressure on the roughness of the indigo film

Topography of indigo films created at five different surface pressures was achieved and compared to each other. The average roughness (Ra) and the root-mean-square roughness (Rq) were summarized at the bottom of Figure 4.16.

Irregular shape of aggregates and a film with uncovered part were found in all images, and a distinctive crystalline structure was not observed. Both

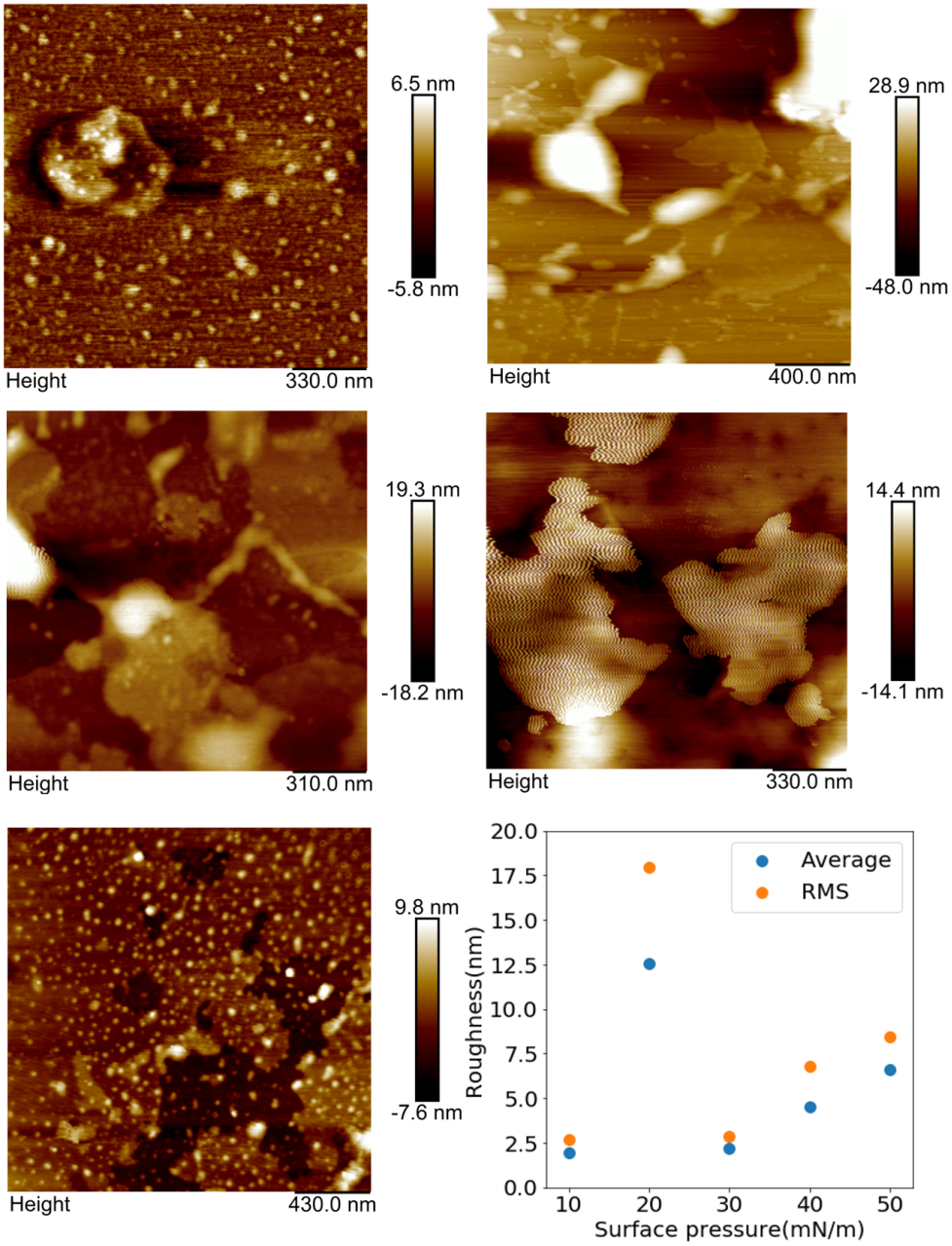

Figure 4.16. AFM images and topography data of indigo films created at different surface pressures. (a) Ra and Rq : 2.0 and 2.7 nm (b) Ra and Rq : 12.5 and 18.0 nm (c) Ra and Rq : 2.2 and 2.84 nm (d) Ra and Rq : 4.5 and 6.8 nm (e) Ra and Rq : 6.6 and 8.4 nm (e) The summary of roughness (blue Ra, orange Rq) and films created at different surface pressure.

Ra and Rq increased as the surface pressure on which the films were created increased. It is capable of comparing the results of the UV-Vis characterization in this study and other studies in the literature survey section with a trend of results of roughness in this section. In UV-Vis characterization in Sec-

tion 4.3.2, indigo film created at lower surface pressure showed the red-shifted max absorbances. Several research groups investigating indigo film mentioned that a bathochromic shift means the evidence of high crystallinity of the indigo film. [11, 70] Therefore, increased roughness with increasing surface pressure may imply that the film is composed of less ordered indigo structure as well as more aggregates in/on the indigo film.

The reason of occurring exception at 20 mN/m might have come from a heterogeneous condition of the film coming from accumulated indigo aggregates. Two regions of intensive accumulation of indigo aggregates were distinguished. One was indigo aggregates were dispersed on the surface in random. The other is a thick indigo band along the droplet on the surface of sample after Langmuir-Schaefer deposition. A water droplet from water subphase can be seen on the sample in Figure 4.17, even though the surface of sample was covered by hydrophobic silane film. Since no external heat energy was provided, these aggregates remained when they were deposited.

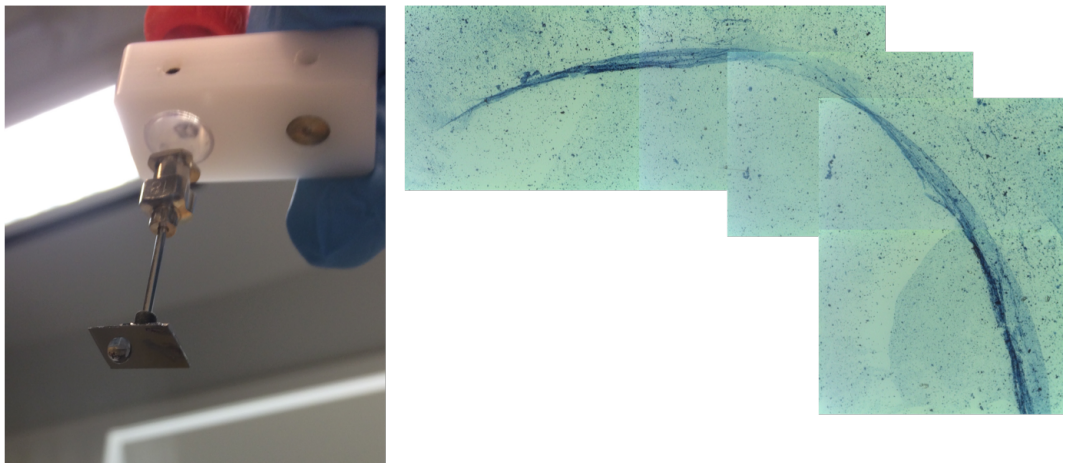

Figure 4.17. (a) Droplet image after deposition. (b) A series of optical microscope images of the mark of the edge of a droplet on the glass substrate.

4.4.4 Effect of the number of deposition cycles on the roughness of the indigo film

Topography of indigo films created at 20 mN/m of surface pressure with different the number of deposition cycles were achieved and compared to each other in Figure 4.18. No significant difference in roughness was observed, However, the sample with five depositions shows fewer valleys compared to the sample with three depositions. It might indicate that additional Langmuir film of indigo onto the Langmuir-Schaefer film of indigo not only filled the space of valleys with its monolayer but also added indigo aggregates. This might be the reason that both indigo films have similar roughness whereas they do not have the similar ratio of valleys and hills.

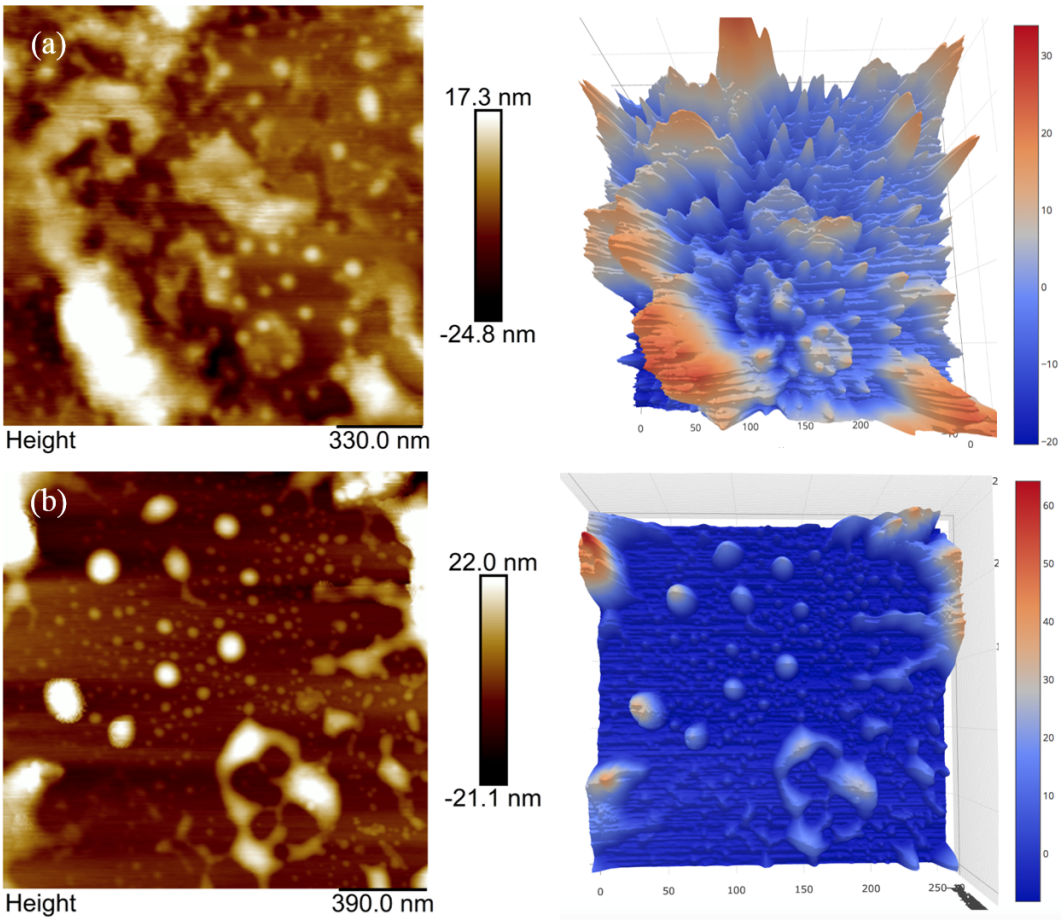

Figure 4.18. (a) The AFM and its corresponding 3D images of an indigo film created at 30mN/m with three deposition. (b) The AFM and its corresponding 3D images of an indigo film created at 30mN/m with five deposition. The AFM images were achieved by a software 'NanoScope Analysis 1.5' and the 3D images were created with a help of visualization tool of plotly by using raw data of indigo films from the AFM images.

Chapter 5

Conclusions

The main purpose of this thesis is to find a possibility of Langmuir-Schaefer deposition for creating the well-ordered structure of the thin film with indigo molecules, which has been highlighted by researchers recently, as a semiconducting layer of organic semiconductor.

This study selected indigo as an organic material and Langmuir-Schaefer as a deposition method based on several reasons. It is known that the structure of a film that has pi-conjugated system strongly affects its performance parameters. Indigo is one of affordable materials consumed for dyeing clothes. Indigo film can offer and advantage that indigo thin film has a more compacted structure with a help of hydrogen bond compared to other organic molecules, which can enhance pi conjugation. Langmuir-Schaefer deposition is known that it has a benefit to create a nanofilm and control its structure.

The hypothesis of this thesis was selected that a Langmuir film of indigo at high surface pressure would create a more ordered Langmuir-Schaefer film on the substrates, and the opposite of the hypothesis that a Langmuir film of indigo at low surface pressure would cause a well-ordered Langmuir-Schaefer film was confirmed.

The major accomplishments are as follows. From a UV-Vis characterization, indigo in solution state showed max absorbance at around 600 nm. New absorbance peak was found at around 700 nm in case of the high concentration of the solution. These results are in accordance with other indigo studies investigated by other researchers. Indigo film displayed the max absorbance red-shifted by 70 nm and decreasing surface pressure and the number of deposition cycles strengthened this trend. So this result confirms the antithesis of the hypothesis that a low surface pressure of Langmuir indigo film has an advantage of creating an ordered indigo film. From an AFM characterization, the thickness of indigo film was revealed around 5 nm, and Most of AFM images found a lot of aggregates with indigo film.

Two insights can be suggested from the accomplishments. One is that Langmuir film at low surface pressure has to be investigated in case non-amphiphilic indigo was selected as a deposition material to produce a well-ordered thin film by Langmuir deposition. The other one is that if the Langmuir-Schaefer film follows the arrangement of Langmuir film, it could mean that a well-ordered the Langmuir film of indigo exists at low surface pressure.

This study has not checked potential parameters affecting the structure of Langmuir film such as the temperature of subphase, the speed of barriers, and the rate of deposition. To achieve accurate information about indigo thin film, XRD characterization on both Langmuir and Langmuir-Schaefer films needs to

be conducted to reveal the structure of the thin films. In addition, it will be useful to create a real organic semiconductor with indigo to check parameters like charge carrier mobility and threshold voltage to verify the effect of using Langmuir deposition for indigo thin film.

Bibliography

[1] Antonio Facchetti. π-conjugated polymers for organic electronics and photovoltaic cell applications. *Chemistry of Materials*, 23(3):733–758, 2010.

[2] Hualong Pan, Yuning Li, Yiliang Wu, Ping Liu, Beng S Ong, Shiping Zhu, and Gu Xu. Low-temperature, solution-processed, high-mobility polymer semiconductors for thin-film transistors. *Journal of the American Chemical Society*, 129(14):4112–4113, 2007.

[3] Prashant Sonar, Samarendra P Singh, Yuning Li, Zi-En Ooi, Tae-jun Ha, Ivy Wong, Mui Siang Soh, and Ananth Dodabalapur. High mobility organic thin film transistor and efficient photovoltaic devices using versatile donor–acceptor polymer semiconductor by molecular design. *Energy & Environmental Science*, 4(6):2288–2296, 2011.

[4] Xugang Guo, Rocio Ponce Ortiz, Yan Zheng, Yan Hu, Yong-Young Noh, Kang-Jun Baeg, Antonio Facchetti, and Tobin J Marks. Bithiophene-imide-based polymeric semiconductors for field-effect transistors: Synthesis, structure- property correlations, charge carrier polarity, and device stability. *Journal of the American Chemical Society*, 133(5):1405–1418, 2011.

[5] Jianhui Hou, Hsiang-Yu Chen, Shaoqing Zhang, Ruby I Chen, Yang Yang, Yue Wu, and Gang Li. Synthesis of a low band gap polymer and its application in highly efficient polymer solar cells. *Journal of the American Chemical Society*, 131(43):15586–15587, 2009.

[6] Itaru Osaka, Toru Abe, Masafumi Shimawaki, Tomoyuki Koganezawa, and Kazuo Takimiya. Naphthodithiophene-based donor–acceptor polymers: versatile semiconductors for ofets and opvs. *ACS Macro Letters*, 1(4):437–440, 2012.

[7] Serap Günes, Helmut Neugebauer, and Niyazi Serdar Sariciftci. Conjugated polymer-based organic solar cells. *Chemical reviews*, 107(4):1324–1338, 2007.

[8] Pierre-Luc T Boudreault, Ahmed Najari, and Mario Leclerc. Processable low-bandgap polymers for photovoltaic applications. *Chemistry of Materials*, 23(3):456–469, 2010.

[9] Kealan J Fallon, Nilushi Wijeyasinghe, Nir Yaacobi-Gross, Raja S Ashraf, David ME Freeman, Robert G Palgrave, Mohammed Al-Hashimi, Tobin J Marks, Iain McCulloch, Thomas D Anthopoulos, et al. A nature-inspired conjugated polymer for high performance transistors and solar cells. *Macromolecules*, 48(15):5148–5154, 2015.

[10] Satej S Dharmapurikar, Arulraj Arulkashmir, Rajashree Y Mahale, and Mrinmoy Kumar Chini. Synthesis of amphiphilic isoindigo co-polymers for organic field effect transistors: A comparative study. *Journal of Applied Polymer Science*, 134(43):45461, 2017.

[11] Eric Daniel Głowacki, Gundula Voss, Lucia Leonat, Mihai Irimia-Vladu, Siegfried Bauer, and Niyazi Serdar Sariciftci. Indigo and tyrian purple–from ancient natural dyes to modern organic semiconductors. *Israel Journal of Chemistry*, 52(6):540–551, 2012.

[12] Matthias Seefelder. *Indigo in culture, science and technology*. ecomed, 1994.

[13] Paul Francis Gordon and Peter Gregory. *Organic chemistry in colour*. Springer Science & Business Media, 2012.

[14] Heinrich Zollinger. *Color chemistry: syntheses, properties, and applications of organic dyes and pigments*. John Wiley & Sons, 2003.

[15] Christopher Cooksey. Tyrian purple: 6, 6'-dibromoindigo and related compounds. *Molecules*, 6(9):736–769, 2001.

[16] Elmar Steingruber. Indigo and indigo colorants. *Ullmann's Encyclopedia of Industrial Chemistry*, 2000.

[17] Eric Daniel Głowacki, Gundula Voss, Kadir Demirak, Marek Havlicek, Nevsal Sünger, Aysu Ceren Okur, Uwe Monkowius, Jacek Gąsiorowski, Lucia Leonat, and Niyazi Serdar Sariciftci. A facile protection–deprotection route for obtaining indigo pigments as thin films and their applications in organic bulk heterojunctions. *Chemical communications*, 49(54):6063–6065, 2013.

[18] Eric Daniel Glowacki, Lucia Leonat, Gundula Voss, Marius Bodea, Zeynep Bozkurt, Mihai Irimia-Vladu, Siegfried Bauer, and Niyazi Serdar Sariciftci. Natural and nature-inspired semiconductors for organic electronics. In *Organic Semiconductors in Sensors and Bioelectronics IV*, volume 8118, page 81180M. International Society for Optics and Photonics, 2011.

[19] Mihai Irimia-Vladu, Eric D Głowacki, Pavel A Troshin, Günther Schwabegger, Lucia Leonat, Diana K Susarova, Olga Krystal, Mujeeb Ullah, Yasin Kanbur, Marius A Bodea, et al. Indigo-a natural pigment for high performance ambipolar organic field effect transistors and circuits. *Advanced Materials*, 24(3):375–380, 2012.

[20] Eric Daniel Głowacki, Lucia Leonat, Gundula Voss, Marius-Aurel Bodea, Zeynep Bozkurt, Alberto Montaigne Ramil, Mihai Irimia-Vladu, Siegfried Bauer, and Niyazi Serdar Sariciftci. Ambipolar organic field effect transistors and inverters with the natural material tyrian purple. *Aip Advances*, 1(4):042132, 2011.

[21] Oratai Pitayatanakul, Kodai Iijima, Tomofumi Kadoya, Minoru Ashizawa, Tadashi Kawamoto, Hidetoshi Matsumoto, and Takehiko Mori. Ambipolar organic field-effect transistors based on indigo derivatives. *Engineering Journal*, 19(3):61–74, 2015.

[22] Sara Bonacchi, Marco Gobbi, Laura Ferlauto, Marc-Antoine Stoeckel, Fabiola Liscio, Silvia Milita, Emanuele Orgiu, and Paolo Samorì. High, anisotropic, and substrate-independent mobility in polymer field-effect transistors based on preassembled semiconducting nanofibrils. *ACS nano*, 11(2):2000–2007, 2017.

[23] Yasin Kanbur, Mihai Irimia-Vladu, Eric D Głowacki, Gundula Voss, Melanie Baumgartner, Günther Schwabegger, Lucia Leonat, Mujeeb Ullah, Hizir Sarica, Sule Erten-Ela, et al. Vacuum-processed polyethylene as a dielectric for low operating voltage organic field effect transistors. *Organic electronics*, 13(5):919–924, 2012.

[24] Eric Daniel Głowacki, Giuseppe Romanazzi, Cigdem Yumusak, Halime Coskun, Uwe Monkowius, Gundula Voss, Max Burian, Rainer T Lechner, Nicola Demitri, Günther J Redhammer, et al. Epindolidiones—versatile and stable hydrogen-bonded pigments for organic field-effect transistors and light-emitting diodes. *Advanced Functional Materials*, 25(5):776–787, 2015.

[25] Chengliang Wang, Huanli Dong, Wenping Hu, Yunqi Liu, and Daoben Zhu. Semiconducting π-conjugated systems in field-effect transistors: a material odyssey of organic electronics. *Chemical Reviews*, 112(4):2208–2267, 2011.

[26] Marta Mas-Torrent and Concepcio Rovira. Novel small molecules for organic field-effect transistors: towards processability and high performance. *Chemical Society Reviews*, 37(4):827–838, 2008.

[27] Daniele Braga and Gilles Horowitz. High-performance organic field-effect transistors. *Advanced materials*, 21(14-15):1473–1486, 2009.

[28] Jana Zaumseil and Henning Sirringhaus. Electron and ambipolar transport in organic field-effect transistors. *Chemical reviews*, 107(4):1296–1323, 2007.

[29] Stefano Casalini, Carlo Augusto Bortolotti, Francesca Leonardi, and Fabio Biscarini. Self-assembled monolayers in organic electronics. *Chemical Society Reviews*, 46(1):40–71, 2017.

[30] Sybille Allard, Michael Forster, Benjamin Souharce, Heiko Thiem, and Ullrich Scherf. Organic semiconductors for solution-processable field-effect transistors (ofets). *Angewandte Chemie International Edition*, 47(22):4070–4098, 2008.

[31] Huanli Dong, Chengliang Wang, and Wenping Hu. High performance organic semiconductors for field-effect transistors. *Chemical Communications*, 46(29):5211–5222, 2010.

[32] Alberto Salleo. Charge transport in polymeric transistors. *Materials Today*, 10(3):38–45, 2007.

[33] Marcel Gsänger, David Bialas, Lizhen Huang, Matthias Stolte, and Frank Würthner. Organic semiconductors based on dyes and color pigments. *Advanced Materials*, 28(19):3615–3645, 2016.

[34] Gerwin H Gelinck, H Edzer A Huitema, Erik van Veenendaal, Eugenio Cantatore, Laurens Schrijnemakers, Jan BPH van der Putten, Tom CT Geuns, Monique Beenhakkers, Jacobus B Giesbers, Bart-Hendrik Huisman, et al. Flexible active-matrix displays and shift registers based on solution-processed organic transistors. *Nature materials*, 3(2):106, 2004.

[35] Edzer Huitema, Gerwin Gelinck, Bas van der Putten, Eugenio Cantatore, Erik van Veenendaal, Laurens Schrijnemakers, B-H Huisman, and Dago de Leeuw. Plastic transistors in active-matrix displays. In *Solid-State Circuits Conference, 2003. Digest of Technical Papers. ISSCC. 2003 IEEE International*, pages 380–381. IEEE, 2003.

[36] John A Rogers, Zhenan Bao, Kirk Baldwin, Ananth Dodabalapur, Brian Crone, VR Raju, Valerie Kuck, Howard Katz, Karl Amundson, Jay Ewing, et al. like electronic displays: Large-area rubber-stamped plastic sheets of electronics and microencapsulated electrophoretic inks. *Proceedings of the National Academy of Sciences*, 98(9):4835–4840, 2001.

[37] Barrett Comiskey, Jonathan D Albert, Hidekazu Yoshizawa, and Joseph Jacobson. An electrophoretic ink for all-printed reflective electronic displays. *Nature*, 394(6690):253, 1998.

[38] Anatoliy N Sokolov, Mark E Roberts, and Zhenan Bao. Fabrication of low-cost electronic biosensors. *Materials today*, 12(9):12–20, 2009.

[39] Bharat Bhushan. *Springer handbook of nanotechnology*. Springer, 2017.

[40] Hwa Sung Lee, Do Hwan Kim, Jeong Ho Cho, Minkyu Hwang, Yunseok Jang, and Kilwon Cho. Effect of the phase states of self-assembled monolayers on pentacene growth and thin-film transistor characteristics. *Journal of the American Chemical Society*, 130(32):10556–10564, 2008.

[41] Malkiat S Johal. *Understanding nanomaterials*. CRC Press, 2012.

[42] J Christopher Love, Lara A Estroff, Jennah K Kriebel, Ralph G Nuzzo, and George M Whitesides. Self-assembled monolayers of thiolates on metals as a form of nanotechnology. *Chemical reviews*, 105(4):1103–1170, 2005.

[43] IH Campbell, S Rubin, TA Zawodzinski, JD Kress, RL Martin, DL Smith, NN Barashkov, and JP Ferraris. Controlling schottky energy barriers in organic electronic devices using self-assembled monolayers. *Physical Review B*, 54(20):R14321, 1996.

[44] Bert de Boer, Afshin Hadipour, M Magdalena Mandoc, Teunis van Woudenbergh, and Paul WM Blom. Tuning of metal work functions with self-assembled monolayers. *Advanced Materials*, 17(5):621–625, 2005.

[45] Robert W Zehner, Bradley F Parsons, Richard P Hsung, and Lawrence R Sita. Tuning the work function of gold with self-assembled monolayers derived from x-[c6h4- c c-] n c6h4- sh (n= 0, 1, 2; x= h, f, ch3, cf3, and och3). *Langmuir*, 15(4):1121–1127, 1999.

[46] Christopher D Zangmeister, Laura B Picraux, Roger D van Zee, Yuxing Yao, and James M Tour. Energy-level alignment and work function shifts for thiol-bound monolayers of conjugated molecules self-assembled on ag, cu, au, and pt. *Chemical physics letters*, 442(4-6):390–393, 2007.

[47] George M Whitesides, Jennah K Kriebel, and Brian T Mayers. Self-assembly and nanostructured materials. In *Nanoscale assembly*, pages 217–239. Springer, 2005.

[48] Christos D Dimitrakopoulos and Patrick RL Malenfant. Organic thin film transistors for large area electronics. *Advanced materials*, 14(2):99–117, 2002.

[49] Y-Y Lin, DJ Gundlach, SF Nelson, and TN Jackson. Stacked pentacene layer organic thin-film transistors with improved characteristics. *IEEE Electron Device Letters*, 18(12):606–608, 1997.

[50] J Takeya, T Nishikawa, T Takenobu, S Kobayashi, Y Iwasa, T Mitani, C Goldmann, Cornelius Krellner, and Bertram Batlogg. Effects of polarized organosilane self-assembled monolayers on organic single-crystal field-effect transistors. *Applied physics letters*, 85(21):5078–5080, 2004.

[51] Yeong Don Park, Jung Ah Lim, Hwa Sung Lee, and Kilwon Cho. Interface engineering in organic transistors. *Materials today*, 10(3):46–54, 2007.

[52] Dae Ho Lee, Taebyoung Oh, and Kilwon Cho. Combined effect of chain length and phase state on adhesion/friction behavior of self-assembled monolayers. *The Journal of Physical Chemistry B*, 109(22):11301–11306, 2005.

[53] Jeong Ho Cho, Dae Ho Lee, Hwa Sung Shin, Sudip K Pattanayek, Chang Y Ryu, and Kilwon Cho. Exploiting poly (dimethylsiloxane)-modified tips to evaluate frictional behavior by friction force microscopy. *Langmuir*, 20(26):11499–11503, 2004.

[54] MC Petty. Possible applications for langmuir-blodgett films. *Thin Solid Films*, 210:417–426, 1992.

[55] Osvaldo N Oliveira Jr. Langmuir-blodgett films-properties and possible applications. *Braz J Phys*, 22(2):60–69, 1992.

[56] Michael C Petty. *Langmuir-Blodgett films: an introduction*. Cambridge University Press, 1996.

[57] A Dhanabalan, DT Balogh, A Riul Jr, JA Giacometti, and ON Oliveira Jr. Langmuir and langmuir–blodgett films of a homopolymer of disperse red-13. *Thin Solid Films*, 323(1-2):257–264, 1998.

[58] CPL Rubinger, RL Moreira, LA Cury, GN Fontes, BRA Neves, A Meneguzzi, and CA Ferreira. Langmuir–blodgett and langmuir–schaefer films of poly (5-amino-1-naphthol) conjugated polymer. *Applied Surface Science*, 253(2):543–548, 2006.

[59] Jian Jin, Lin Song Li, Yi Li, Yan Jie Zhang, Xia Chen, Dejun Wang, Shimei Jiang, Tie Jin Li, Liang Bing Gan, and Chun Hui Huang. Structural characterizations of c60-derivative langmuir- blodgett films and their photovoltaic behaviors. *Langmuir*, 15(13):4565–4569, 1999.

[60] Jean-Louis Gallani, Delphine Felder, Daniel Guillon, Benoît Heinrich, and Jean-François Nierengarten. Micelle formation in langmuir films of c60 derivatives. *Langmuir*, 18(7):2908–2913, 2002.

[61] Luis Serrano-Andrés and Björn O Roos. A theoretical study of the indigoid dyes and their chromophore. *Chemistry–A European Journal*, 3(5):717–725, 1997.

[62] M Klessinger and W Lüttke. Theoretische und spektroskopische untersuchungen an indigo-farbstoffen—ii: Das chromophore system der indigofarbstoffe. *Tetrahedron*, 19:315–335, 1963.

[63] John Griffiths. *Colour and constitution of organic molecules*. Academic press, 1976.

[64] Jürgen Fabian and Horst Hartmann. *Light absorption of organic colorants: theoretical treatment and empirical rules*, volume 12. Springer Science & Business Media, 2013.

[65] Kichisuke Nishimoto. A mo theoretical study of organic dyes i. effect of chemical softness on the electronic spectra. *Bulletin of the Chemical Society of Japan*, 66(7):1876–1880, 1993.

[66] Denis Jacquemin, Julien Preat, Valérie Wathelet, and Eric A Perpète. Substitution and chemical environment effects on the absorption spectrum of indigo. *The Journal of chemical physics*, 124(7):074104, 2006.

[67] Anna Amat, Francesca Rosi, Costanza Miliani, Antonio Sgamellotti, and Simona Fantacci. Theoretical and experimental investigation on the spectroscopic properties of indigo dye. *Journal of Molecular Structure*, 993(1-3):43–51, 2011.

[68] Alan R Monahan and James E Kuder. Spectroscopic differences between crystalline and amorphous phases of indigo. *The Journal of Organic Chemistry*, 37(25):4182–4184, 1972.

[69] Julius Weinstein and George M Wyman. Spectroscopic studies on dyes. i. the association of indigo dyes in the solid phase1. *Journal of the American Chemical Society*, 78(11):2387–2390, 1956.

[70] Peter W Sadler and Reginald L Warren. Synthesis and absorption spectra of the symmetrical chloroindingos. *Journal of the American Chemical Society*, 78(6):1251–1255, 1956.

[71] Eric Daniel Głowacki, Gundula Voss, and Niyazi Serdar Sariciftci. 25th anniversary article: progress in chemistry and applications of functional indigos for organic electronics. *Advanced Materials*, 25(47):6783–6800, 2013.

[72] Eric Daniel Głowacki, Mihai Irimia-Vladu, Martin Kaltenbrunner, Jacek Gsiorowski, Matthew S White, Uwe Monkowius, Giuseppe Romanazzi, Gian Paolo Suranna, Piero Mastrorilli, Tsuyoshi Sekitani, et al. Hydrogen-bonded semiconducting pigments for air-stable field-effect transistors. *Advanced Materials*, 25(11):1563–1569, 2013.

[73] Paolo Bertoncello, Andrea Notargiacomo, and Claudio Nicolini. Synthesis, fabrication and characterization of poly [3-3 (vinylcarbazole)](pvk) langmuir–schaefer films. *Polymer*, 45(5):1659–1664, 2004.

[74] Alexey S Sizov, Elena V Agina, Fatemeh Gholamrezaie, Vladimir V Bruevich, Oleg V Borshchev, Dmitry Yu Paraschuk, Dago M de Leeuw, and Sergey A Ponomarenko. Oligothiophene-based monolayer field-effect transistors prepared by langmuir-blodgett technique. *Applied Physics Letters*, 103(4):134_1, 2013.

[75] Matthias Lessel, Oliver Bäumchen, Mischa Klos, Hendrik Hähl, Renate Fetzer, Michael Paulus, Ralf Seemann, and Karin Jacobs. Self-assembled silane monolayers: an efficient step-by-step recipe for high-quality, low energy surfaces. *Surface and Interface Analysis*, 47(5):557–564, 2015.

[76] Yang Leng. *Materials characterization: introduction to microscopic and spectroscopic methods*. John Wiley & Sons, 2009.

[77] Heinz-Helmut Perkampus. *UV-VIS Spectroscopy and its Applications*. Springer Science & Business Media, 2013.

[78] C Miliani, A Romani, and G Favaro. A spectrophotometric and fluorimetric study of some anthraquinoid and indigoid colorants used in artistic paintings. *Spectrochimica Acta Part A: Molecular and Biomolecular Spectroscopy*, 54(4):581–588, 1998.

[79] PW Sadler. Absorption spectra of indigoid dyes. *The Journal of Organic Chemistry*, 21(3):316–318, 1956.

[80] Douglas A Skoog, Donald M West, F James Holler, and Stanley Crouch. *Fundamentals of analytical chemistry*. Nelson Education, 2013.

[81] MN Berberan-Santos. Beer's law revisited. *Journal of Chemical Education*, 67(9):757, 1990.

[82] Pernilla Wittung, Johan Kajanus, Mikael Kubista, and Bo G Malmström. Absorption flattening in the optical spectra of liposome-entrapped substances. *FEBS letters*, 352(1):37–40, 1994.

[83] Belinda Heyne. Self-assembly of organic dyes in supramolecular aggregates. *Photochemical & Photobiological Sciences*, 15(9):1103–1114, 2016.

[84] Peter Süsse, Manfred Steins, and Vladimir Kupcik. Indigo: Crystal structure refinement based on synchrotron data. *Zeitschrift für Kristallographie-Crystalline Materials*, 184(1-4):269–274, 1988.

[85] H von Eller-Pandraud. Structure cristalline de l'isoindigo. *Acta Crystallographica*, 13(11):936–938, 1960.

[86] Robin JH Clark and Christopher J Cooksey. Monobromoindigos: a new general synthesis, the characterization of all four isomers and an investigation into the purple colour of 6, 6-dibromoindigo. *New Journal of Chemistry*, 23(3):323–328, 1999.

[87] RRL De Oliveira, DAC Albuquerque, TGS Cruz, FM Yamaji, and FL Leite. Measurement of the nanoscale roughness by atomic force microscopy: basic principles and applications. In *Atomic force microscopy-imaging, measuring and manipulating surfaces at the atomic scale*. InTech, 2012.

[88] Yuliang Wang and Marya Lieberman. Growth of ultrasmooth octadecyltrichlorosilane self-assembled monolayers on sio2. *Langmuir*, 19(4):1159–1167, 2003.